Journal Pre-proof

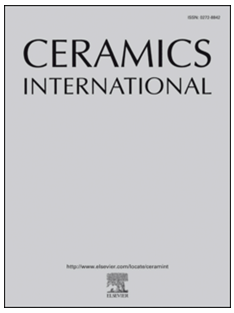

MnO_2-TiO_2 Composite Additives Driven Low-Cost Fabrication of Coal Gangue/ Bauxite Ceramic Proppants

Heng Zhang, Tian Yuan, Liehui Zhang, Zhaozhong Yang, Xiaogang Li, Fatereh Dorosti, Jingyi Zhu, Jin Zhang, Hongcheng Yang, Hao Wang, Lei Ge

PII: S0272-8842(25)03039-1

DOI: https://doi.org/10.1016/j.ceramint.2025.06.353

Reference: CERI 47567

To appear in: *Ceramics International*

Received Date: 1 April 2025

Revised Date: 8 June 2025

Accepted Date: 24 June 2025

Please cite this article as: H. Zhang, T. Yuan, L. Zhang, Z. Yang, X. Li, F. Dorosti, J. Zhu, J. Zhang, H. Yang, H. Wang, L. Ge, MnO_2-TiO_2 Composite Additives Driven Low-Cost Fabrication of Coal Gangue/ Bauxite Ceramic Proppants, *Ceramics International*, https://doi.org/10.1016/j.ceramint.2025.06.353.

MnO_2-TiO_2 Composite Additives Driven Low-Cost Fabrication of Coal Gangue/Bauxite Ceramic Proppants

Heng Zhang [a], Tian Yuan [a], Liehui Zhang [b], Zhaozhong Yang [b], Xiaogang Li [b], Fatereh Dorosti [c], Jingyi Zhu [b], Jin Zhang [a,*], Hongcheng Yang [a], Hao Wang [c], Lei Ge [c*]

[a] School of New Energy and Materials, Southwest Petroleum University, Chengdu 610500, China;
[b] National Key Laboratory of Reservoir Geology and Development Engineering, Southwest Petroleum University, Chengdu, Sichuan 610500, China
c School of Engineering, Centre for Future Materials, University of Southern Queensland, Springfield, QLD 4300, Australia.
* Corresponding e-mail: jzhang@swpu.edu.cn (JZ); lei.ge@unisq.edu.au (LG)

Abstract: The urgency of resource utilization for coal gangue has driven innovations toward its high-value processing technologies. Although coal gangue can serve as a low-cost source of silicon and aluminum—reducing raw material costs by 14% compared to pure bauxite—its direct application in the production of ceramic proppants faces significant challenges. These challenges include an excessively high calcination temperature (e.g. >1450 °C) and compromised mechanical properties. In this study, we designed the fabrication of ceramic proppants by using coal gangue and bauxite as raw materials. By adjusting the dosage of a MnO_2–TiO_2 composite additive (0–7.5 wt%), a dual-phase ceramic proppant composed of corundum and mullite was prepared. The results show that the addition of the MnO_2–TiO_2 can lower the sintering temperature, allowing the proppant to develop a well-dense structure within the temperature range of 1250 to 1350 °C. However, the composite additive also inhibits the formation of mullite while promoting the development of the corundum phase. This phase transformation

enhances the compressive strength of the proppant but simultaneously increases its density. When the composite additive content is 7.5 wt% and the sintering temperature is 1350 °C, the resulting ceramic proppant exhibits a bulk density of 1.88 ± 0.01 g/cm³ and an apparent density of 3.17 ± 0.02 g/cm³, with a minimum breakage rate of 2.71 ± 0.32% under 52 MPa.

Keywords: Ceramic proppants; Bauxite; Coal gangue; Composite additives; Sintering

1. Introduction

Shale gas reservoirs consist of a matrix and natural fractures, characterized by extremely low permeability. Therefore, horizontal well hydraulic fracturing has become the predominant method for exploiting shale gas reservoirs [1]. Proppants play a crucial role in this process by preventing fracture closure and ensuring sustained high production of shale gas, oil, and gas resources [2]. In 1947, quartz sand was used for the first time as a proppant material, and it was widely adopted due to its low cost and low density [3]. However, since quartz sand has relatively low compressive strength, it is only suitable for service environments where the closure stress is below 28 MPa [4], which severely limits its application. To enhance the compressive strength and overall performance of proppants, two new types of proppants—polymer-coated and ceramic —have been developed successively since the 1980s [5]. Polymer-coated proppants are produced by coating traditional proppants with polymers, offering advantages such as low density, high compressive strength, and excellent flow conductivity. However, under high-

temperature and high-pressure conditions, their fracture permeability is significantly reduced, thus limiting their application in deep reservoirs [6]. Ceramic proppants, on the other hand, are artificial fracturing proppants manufactured by granulating aluminosilicate raw materials followed by high-temperature sintering. They possess high strength, high sphericity, and chemical stability, making them ideal for fracturing in unconventional reservoirs. Nevertheless, their production still faces challenges such as high sintering temperatures and high production costs [7].

China's unconventional oil and gas resources are abundant, but the reservoirs have complex structures and are difficult to exploit, which imposes higher demands on the mechanical properties and conductivity of proppants [8]. In addition, the mining and transportation costs of bauxite have been rising in recent years, which limits its application in large-scale ceramic proppant production. To overcome the resource and cost limitations, many researchers have explored the use of solid waste to replace bauxite, such as oil-based drilling cuttings [9], fly ash [10], coal gangue, and waste ceramic sand [11]. Moreover, some studies have begun to focus on utilizing biomass materials, such as rice husk ash [12], to develop low-cost, high-performance ceramic proppants. This approach not only helps reduce the environmental pollution caused by solid waste but also promotes the secondary utilization of resources.

Coal gangue, an industrial solid waste generated during coal production, mainly consists of Al_2O_3 and SiO_2, which are similar to the composition of bauxite [13]. Numerous studies have explored the process of using coal gangue to partially replace bauxite in the

preparation of ceramic proppants [14]. However, the ceramic proppants produced using coal gangue still face challenges such as low compressive strength and high sintering temperatures. Lei et al. [15] replaced bauxite with 20 wt% coal gangue and added 20 wt% potassium feldspar as an additive; the proppants sintered at 1260 °C exhibited a breakage rate of 5.12% under 28 MPa. To further increase the coal gangue content, Zhao et al.[16] used 40 wt% coal gangues; under a sintering temperature of 1450 °C, the ceramic proppants achieved a minimum breakage rate of 7.0% under 35 MPa. Subsequently, Hao et al.[17] found that at the same sintering temperature, increasing coal gangue content results in a reduced apparent density and a significant decline in the compressive strength of the ceramic proppants. Most studies indicate that when the coal gangue content exceeds 30 wt%, the proppants can withstand closure stresses of only up to 35 MPa [18].To address these issues, researchers have proposed various strategies to enhance the compressive strength of ceramic proppants and reduce the sintering temperature, among which the use of additives has received considerable attention. The commonly used additives are mainly divided into high-temperature liquid-phase sintering aids (such as MgO [19] and CaO [20]) and lattice distortion sintering aids (such as Fe_2O_3 [21], V_2O_5 [22], TiO_2 [23], and MnO_2 [24]). Studies have shown that the incorporation of additives can effectively reduce the formation temperature of the ceramics and enhance grain growth. For example, the addition of 5 wt% $CaCO_3$ at 1350 °C generates a large amount of liquid phase, leading to a change in the mass transfer mode, which in turn promotes the growth of mullite grains and sintering densification [25]. In addition, MnO_2 and TiO_2 not only reduce the formation

temperature of mullite but also improve the mechanical properties of ceramics [26][27]. Moontoya et al.[28] suggested that the enhancement of the mechanical properties of alumina-mullite ceramics by TiO_2 could be attributed to the incorporation of Ti^{4+} ions into the secondary mullite phase, which promotes nucleation and crystal growth. Chen et al.[29] found that TiO_2 can significantly enhance the compressive strength by forming an interlocking rod-like mullite structure; however, when its content reaches 6 wt%, the increase in the glassy phase leads to a higher breakage rate. Furthermore, Lahiri et al.[30] compared the applications of MgO and TiO_2 in alumina ceramics and found that titanium oxide forms a solid solution in Al_2O_3, thus enhancing the densification of α-alumina and promoting grain growth, while magnesium oxide forms magnesium aluminate spinel with alumina at low temperatures, which has less impact on densification and grain growth. Yang et al.[31] discovered that the introduction of MnO_2 in silicate systems not only effectively lowers the formation temperature of mullite, promoting the nucleation and growth of mullite whiskers at low temperatures but also suppresses the abnormal grain growth during low-temperature sintering. Additionally, Majidian et al.[32] introduced manganese oxide as an additive in alumina-mullite-zirconia composite ceramics and found that manganese forms a solid solution in alumina, thereby promoting densification and enhancing the mechanical properties of the ceramics. However, the addition of MnO_2 was also observed to delay the formation of the mullite phase. Although a single additive can improve performance to some extent, the use of composite additives can exert a synergistic effect to further promote sintering densification and enhance mechanical

properties. Gnanasagaran et al. [33] added TiO_2 and MnO_2 to Al_2O_3 ceramics, and after sintering at 1250–1300 °C, a relative density of up to 98% was achieved. In mullite-corundum ceramics, Liu et al. [34] used MnO_2 and CaO as composite additives and found that the composite system was more effective than using CaO alone in reducing the sintering temperature and enhancing the compressive strength; ceramic proppants prepared at 1200 °C exhibited a breakage rate of 2.2–4.5% under 69 MPa. Similarly, Wang et al. [35] employed K_2O and P_2O_5 as composite additives, which transformed the mullite morphology from equiaxed grains to needle-like and columnar forms; compared with single additives, the composite additives increased the system's liquid phase by 2 wt%. In summary, compared to single additives, composite additives show significant advantages in enhancing the structure and mechanical properties of ceramic proppants. However, there are still few reports on incorporating TiO_2 and MnO_2 as composite additives in the preparation of bauxite–coal gangue ceramic proppants. Further exploration of their application potential for performance optimization and cost control is of great significance.

This study applied a composite additive strategy to prepare ceramic proppants from silicon-rich aluminous coal gangue waste (see Figure 1), promoting the high-value utilization of solid waste resources. Pre-calcined coal gangue and pre-mixed bauxite were used as the base materials to tailor the physical and chemical properties of the ceramic proppants. MnO_2 and TiO_2 were selected as composite additives. The effects of coal gangue pre-calcination, sintering temperature, and composite additives on the phase

composition, microstructure, and mechanical properties of the ceramic proppants were systematically investigated. In addition, an evaluation of the proppant production cost was conducted to assess the economic feasibility of the process.

2. Experimental Section

2.1. Experimental Materials

The skeletal materials used included clinker bauxite (300 mesh, Henan Borun Foundry Materials Co., Ltd.) and coal gangue (300 mesh, Shanxi Changqing Petroleum Fracturing Proppant Co., Ltd.), with their specific chemical compositions listed in

Table 1 Chemical Composition of Raw Materials (wt%). The additives included MnO_2 (analytical grade, Chengdu Kelong Chemical Reagent Factory) and TiO_2 (analytical grade Chengdu Kelong Chemical Reagent Factory). Polyvinyl alcohol (PVA, AR, Chengdu Kelong Chemical Reagent Factory) was used as the binder.

2.2. Preparation Process

Table S1 lists the composition ratios of different proppant samples. Samples Z1-Z4 were sintered at a fixed temperature of 1450 °C with composite additive content ranging from 0 to 7.5 wt%. Samples Z5-Z8 maintained a fixed composite additive content of 7.5 wt%, with sintering temperatures ranging from 1250 to 1400 °C. Based on literature research[36],

when the coal gangue content exceeds 30%, the mullite phase inside the ceramic proppant grows abnormally, accompanied by pore formation, leading to an increased breakage rate. Therefore, in this study, the mass ratio of bauxite to coal gangue in the framework material was fixed at 7:3, and the mass ratio of MnO_2 to TiO_2 in the composite additive was fixed at 3:1.The raw materials were wet-milled using a planetary ball mill (QM-QX04, Zhejiang Jiechen Instrument Equipment Co., Ltd.) at a rotational speed of 400 r/min for 4 hours, with a mass ratio of powder, grinding balls, and deionized water set at 1:1:1. The milled slurry was dried at 120 °C for 24 hours in an electric blast drying oven (101A-2ET, Shanghai Experimental Instrument Factory Co., Ltd.). The dried lumps were ground and sieved through a 350-mesh (40 μm) screen. A laser particle size analyzer (Masterizer-2000, Malvern Instruments Ltd) was used to measure the particle size distribution (Fig. S1), revealing a bimodal distribution with an average particle size D_{50} of 2.828 μm. The appropriate amount of powder was placed into a sugar-coating machine (BY-300A, Guangzhou Daxiang Electronic Machinery Equipment Co., Ltd.) for granulation at a rotational speed of 50 r/min. During the process, 1.5 wt% PVA solution and powder were continuously added until the granules grew to the target size. Ceramic proppant green pellets of 30-50 mesh were selected and sintered in a tubular furnace (STG-60-17, Henan Sante Furnace Technology Co., Ltd.). The sintering process involves heating at 5 °C/min from room temperature to 1000 °C, followed by 3 °C/min from 1000 °C to the final sintering temperature, with a holding time of 90 minutes at the final temperature. The preparation process is shown in Fig. S2.

2.3. Characterization

Chemical composition analysis of major oxides in bauxite, raw coal gangue, and calcined coal gangue was performed using X-ray fluorescence spectroscopy (Bruker S8 TIGER, Bruker AXS GmbH). The pyrolysis characteristics of coal gangue were investigated via thermogravimetric-differential scanning calorimetry (TG-DSC, NETZSCH STA 449F3) under an air atmosphere with a heating rate of 10 °C/min from 30 °C to 1200 °C. The phase composition of the samples was analyzed by X-ray diffraction (XRD, DX-2007B, Dandong Haoyuan Instrument Co., Ltd.) with a scanning range of 10° to 80° (2θ) at a step size of 0.02°. The phase identification and semi-quantitative phase analysis were performed using X'pert HighScore software. Fourier transform infrared spectroscopy (FTIR) was employed to analyze the Z1 and Z5 ceramic proppant samples for the characterization of chemical bonds within the proppants. Macroscopic morphology of proppants was observed through a stereomicroscope (SZM7045, Sunny Optical Technology Co., Ltd.), while cross-sectional microstructure and elemental composition were characterized by field-emission scanning electron microscopy (FE-SEM, Thermo Scientific Apreo 2) coupled with energy-dispersive spectroscopy (EDS, OXFORD ULTIM Max65). Key performance parameters including sphericity, bulk density, apparent density, and breakage ratio under 52 MPa closure stress were measured by the Chinese Petroleum Industry Standard SY/T 5108-2014.

3. Results and Discussion

3.1. Raw Material Analysis

Figure 2 shows the TG–DSC results of coal gangue over the temperature range of 30 °C to 1200 °C, alongside the XRD patterns of coal gangue before and afte r calcination as well as the XRD pattern of bauxite. The TG–DSC data (Figure 2(a)) indicate that in the range of 30–290 °C, the coal gangue loses about 1.86% of its mass, mainly due to the evaporation of free water and the oxidative deco mposition of organic matter. When the temperature increases to 300–610 °C, a m ore significant weight loss of approximately 17.75% occurs. Chemical compositio n analysis of coal gangue indicates the presence of combustible components, incl uding carbon and sulfur, which oxidize within the temperature ranges of 500–600 °C and 450–800 °C, respectively. This stage involves the oxidation of both carbo n and sulfur [37]. Based on the XRD analysis of coal gangue before and after ca lcination (see Figure 2(b and c)), this stage can be attributed to the thermal dec omposition of kaolinite, leading to the release of hydroxyl groups from kaolinite followed by its transformation into metakaolin and the oxidation of FeS_2[38]. The reaction equations (1) and (2) illustrate these processes, which are manifested as endothermic peaks at 454 °C and an exothermic peak at 500 °C on the DSC cur ve respectively. Regarding the formation mechanism of the endothermic peak at 545 °C, two possible explanations have been proposed: it may result either from the gasification reaction of residual carbon components or the reorganization of t

he short-range ordered structure within metakaolin [39]. Beyond 610 °C, the TG c urve gradually declines, which is attributed to the decomposition of inorganic mi nerals and the residual organic components [40]. Analysis of the TG curve reveals that most volatile substances in the coal gangue have decomposed before reachi ng 700 °C, thereby reducing their impact on the densification of the ceramic gra nule proppant. Therefore, 700 °C was chosen as the calcination temperature for t he coal gangue in this study.

$$Al_2O_3 \cdot 2SiO_2 \cdot 2H_2O(Kaolinite) \rightarrow Al_2O_3 \cdot 2SiO_2(Metakaolin) + 2H_2O \quad (1)$$

$$4FeS_2 + 11O_2 \rightarrow 2Fe_2O_3 + 8SO_2 \quad (2)$$

After calcination, the ratio of Al_2O_3 to SiO_2 in the coal gangue is 0.826 (see Table 1), which is higher than that of the raw coal gangue. Figure 2b shows the XRD pattern of the raw coal gangue, where the main phases are quartz, kaolinite, and pyrite. Figure 2(c) presents the XRD pattern of the coal gangue calcined at 700 °C for 1 hour, revealing quartz as the dominant phase along with diffraction peaks corresponding to residual kaolinite and hematite. By comparing the XRD patterns before and after calcination, it can be observed that the diffraction peak of kaolinite at 12.46° disappears, indicating that the structure of the coal gangue has been disrupted and that kaolinite has transformed into metakaolin. In addition, the relative intensities of the remaining kaolinite diffraction peaks are significantly reduced, indicating that a large amount of kaolinite has

decomposed[41]. XRD pattern of the clinker bauxite shows that corundum and mullite are its primary crystalline phase. (Figure 2d).

3.2. The Effect of Composite Additive Content on Ceramic Proppants

The effect of composite additives on the microstructure and mechanical properties of the ceramic proppant was investigated at the sintering temperature of 1450 °C. The resulting ceramic proppants were designated as Z1 to Z4, with the MnO_2/TiO_2 composite additive added at ratios of 0, 2.5, 5, and 7.5 wt%, respectively.

Figure 3 displays photographs of the ceramic proppants prepared with different additive contents. As the additive content increases, the color of the proppants changes gradually from light yellow to dark gray, and their average diameter is approximately 446.85 μm. The sphericity of the proppants was evaluated using the Krumbein/Slos template method[42], as shown in Figure 3. The results indicate that the average sphericity of the proppants exceeds 0.9, which satisfactorily meets the requirements of the oil and gas industry standard SY/T5108-2014. However, when the additive content is increased to 7.5 wt% and sintered at 1450 °C, severe agglomeration occurs on the particle surfaces, resulting in poor particle dispersion (see Figure 3). Analysis suggests that this phenomenon is due to the excessive additive content (7.5 wt%) at this temperature, which produces a large amount of liquid phase during high-temperature sintering, causing the particles to stick together. Therefore, for the ceramic proppants prepared with this formulation at 1450 °C, only XRD analysis was performed, and no further evaluation of other properties was conducted.

Figure 4 presents the XRD patterns of the ceramic proppants prepared with different additive contents at a sintering temperature of 1450 °C, along with the semi-quantitative analysis and FWHM (full width at half maximum) analysis results of the mullite and corundum phases. From Figure 4, it can be observed that the main diffraction peaks correspond to the corundum phase (PDF#00-046-1212) and the mullite phase (PDF#01-015-0776). Although the XRD patterns of the proppants prepared with different additive contents are similar, there are significant differences in the diffraction peak intensities. Analysis indicates that the diffraction peak intensity of the corundum phase gradually increases with increasing additive content, while that of the mullite phase decreases. Semi-quantitative analysis using HishScore software (Figure 4b) confirms this trend, showing a clear decrease in mullite content and a corresponding increase in corundum. This phenomenon is likely due to enhanced glass phase formation induced by the additives, which consumes more Si and thus reduces the availability of Si for mullite crystallization. Furthermore, FTIR and EDS mapping analyses of Z1 and Z5 samples before and after corrosion (see Fig.S3 to S7) suggest that increased Mn content may interfere with the participation of Si in mullite formation, further contributing to the observed reduction in mullite phase.

Further analysis shows that the mullite and corundum phases exhibit their strongest diffraction peaks at the (210) and (104) planes, respectively. The FWHM reflects the crystallinity of the crystals, where a smaller FWHM corresponds to higher crystallinity. By analyzing the FWHM of the mullite (210) and corundum (104) phases in the ceramic

proppants prepared with different additive contents (see Figure 4(c) and 4(d)), the anisotropy of crystal growth can be inferred[19]. As shown in Figure 4(c) and 4(d), with 2.5 wt% additive content, the FWHM of mullite at the (110) plane and corundum at the (104) and (113) planes narrow, indicating improved crystallinity of mullite at (110) and corundum at (104). However, when the additive content rises to 7.5 wt%, the FWHM of mullite at the (210) plane widens, suggesting that the 7.5 wt% additive restricts the crystallization of mullite at the (210) plane. At the same time, the FWHM of mullite at the (110) plane and corundum at the (104) plane reduces significantly, indicating enhanced crystal growth in these specific planes.

Figure 5(a-b) shows the cross-sectional microstructures of the ceramic proppants prepared under a sintering temperature of 1450 °C with different additive contents, along with the curves of bulk density, apparent density, and breakage rate. According to Figure 5 (Z1a and Z1 b), the cross-section of the Z1 proppant (without additives) exhibits numerous irregulars, interconnected pores, and a distinct layered structure, lacking a dense structure. Pore size analysis was performed using ImageJ Pro Plus software, where the black areas represent the pores, with pore sizes ranging from 2.5 to 18 μm, as shown in Fig. S8. This indicates that when no additive is incorporated, a minimal liquid phase is generated to effectively fill the internal pores of the ceramic proppant, resulting in low bulk and apparent densities and a high breakage rate of 20.7%. When 2.5 wt% of the composite additive is added, the cross-section of the Z2 proppant displays a well-densified outer layer with only a few small pores, while the central region still contains

larger pores, with sizes ranging from 0.2 to 20 μm. This may be due to the inadequate binding between the mother pellet and the later-added powder during granulation. Compared to the Z1 proppant, the Z2 proppant shows a significant increase in both bulk density and apparent density. Within the Z2 proppant, an interwoven structure of rod-shaped mullite and alumina particles is formed, which further enhances its compressive strength and markedly reduces the breakage rate. After adding 5 wt% of the composite additive, the cross-sectional center of the Z3 proppant still contains large pores, and, compared to the Z2 proppant, the number of pores in the outer region increases noticeably. This is possibly attributed to the coarsening of mullite, which leads to an insufficient filling of the pores by the liquid phase, thereby creating more pores [43]. Consequently, both the bulk and apparent densities slightly decrease. Although the interlocking structure of blocky Al_2O_3 particles with rod-shaped mullite is more pronounced in the Z3 proppant, the increased formation of low-strength glass phase and associated pore development caused by the 5 wt% additive leads to a reduction in compressive strength. In summary, at 1450 °C, the ceramic proppant prepared with 2.5 wt% composite additive exhibits the best performance, with a breakage rate of 3.13 ± 0.33% under 52 MPa, and apparent density and bulk density of 3.26 ± 0.02 g/cm³ and 1.85 ± 0.02 g/cm³, respectively.

3.3. The Effect of Sintering Temperature on the Performance of Ceramic Proppants

Analysis of Figure 4 shows that increasing the composite additive content promotes the formation of the corundum phase, which exhibits higher diffraction intensity than the

mullite phase. Therefore, to further enhance the compressive strength of the ceramic proppants, the maximum composite additive content in this section is set to 7.5 wt%. In addition, the sintering temperature is also one of the important factors affecting the performance of the ceramic proppants. As shown in Figure 3(d), when the sintering temperature is 1450 °C and the composite additive content is 7.5 wt%, the ceramic granules tend to stick together, making it impossible to effectively evaluate and analyze their performance. Hence, in this section, to study the effects of different sintering temperatures on the structure and performance of the ceramic proppants, the sintering temperatures are set to 1250, 1300, 1350, and 1400 °C, and the four proppants are designated as Z5–Z8.

Figure 6 presents the XRD patterns of the ceramic proppants prepared with a 7.5 wt% additive content under different sintering temperatures, along with the semi-quantitative analysis and FWHM (full width at half maximum) analysis results of the mullite and corundum phases. Analysis of Figure 6(a) reveals that the main phases in all samples are the corundum phase (PDF#00-046-1212) and the mullite phase (PDF#01-015-0776), with a consistent phase composition. This indicates that variations in sintering temperature between 1250 and 1400 °C do not significantly affect the types of phases present. As the sintering temperature increases from 1250 °C to 1400 °C, the diffraction peak intensities of both the corundum and mullite phases gradually increase, suggesting that the reaction between quartz and corundum becomes more complete, with a slight increase in mullite formation (see Figure 6b). Combined with the FWHM analysis (Figure 6(c and d)), it can

be seen that at a sintering temperature of 1350 °C, the FWHM of mullite at the (110) plane is smaller than that at the (210) plane, suggesting a faster crystal growth rate along the (110) plane compared to the (210) plane. However, when the sintering temperature is further increased to 1400 °C, the FWHM of mullite at the (210) plane decreases significantly, which indicates that a higher sintering temperature favors the growth of mullite on the (210) plane. The preferentially oriented growth of mullite crystals under different sintering temperatures leads to distinct crystal morphologies [44].

Figure 7(a-b) shows the cross-sectional microstructures of the ceramic proppants prepared at different sintering temperatures with an additive content of 7.5 wt%, as well as the corresponding curves of bulk density, apparent density, and breakage rate. At a sintering temperature of 1250 °C, the Z5 ceramic proppant exhibits a uniformly distributed porous internal structure, leading to reduced bulk and apparent densities. At this temperature, the reaction forming mullite is incomplete, and a complete rod-like mullite network structure is not established, leading to a relatively high breakage rate; however, the breakage rate still meets the industry standard for oil and gas proppants (<9%). When the sintering temperature is raised to 1300 °C, the pores inside the Z6 ceramic proppant are significantly reduced (see Figure 7(Z6a and Z6b)), and the bulk density, apparent density, and compressive strength are all improved. Further increasing the sintering temperature to 1350 °C leads to forming a liquid phase that fills the pores. The Z7 ceramic proppant exhibits a more compact structure, and the internal pore morphology reveals that rod-like mullite continues to grow and interlock with blocky

Al_2O_3 , forming a tightly interwoven network that significantly enhances the compressive strength of the matrix [45]. When the sintering temperature reaches 1400 °C, the number of pores inside the ceramic proppant increases and their diameters become noticeably larger, with a maximum of 14 μm, as shown in Fig. S9, causing a decline in bulk density. This phenomenon may be attributed to thermal stress, which leads to the migration and reorganization of the internal gas pore positions, forming new, larger pores. In addition, the aspect ratio of the rod-like mullite decreases (see Fig. S10), and it adheres to the glassy phase, resulting in the deformation of the original mullite network structure and an increase in the breakage rate [46]. This study found that the ceramic proppant prepared with 7.5 wt% composite additive at 1350 °C exhibited the best overall performance, with an apparent density of 3.17 ± 0.02 g/cm³, a bulk density of 1.88 ± 0.01 g/cm³, and a breakage rate of 2.71 ± 0.32% under 52 MPa, all by the SY/T5108-2014 standard.

To better observe the internal crystal morphology of the ceramic proppant, the cross-section of the proppant was subjected to acid etching using 3% HF acid. Figure 8 shows the SEM micrographs and EDS elemental analysis of the Z7 proppant after HF etching. As seen in Figure 8(a), the internal crystal morphology of the proppant mainly exhibits blocky, granular, and rod-like forms. In the blocky crystals, only Al and O are detected (see Figure 8b), indicating that the blocky morphology corresponds to corundum. Analysis of Figures 8(c and d) shows that the rod-like and granular morphologies correspond to mullite. However, the atomic ratios of Al, Si, and O in these two forms deviate significantly from the theoretical atomic ratio of mullite (6:2:13), which is mainly

attributed to the low yield and incomplete crystal development of mullite during sintering at 1350 °C [44]. According to relevant literature [47], granular mullite is regarded as secondary mullite, possibly formed through mutual diffusion between the glassy phase and Al_2O_3 particles, resulting in its deposition on their surfaces. Further elemental analysis reveals that the Ti content in both the rod-like mullite and secondary mullite is much higher than the Mn content. This difference is related to the incorporation of Ti^{4+} into two different distorted octahedral sites, leading to a higher Ti^{4+} content in the mullite structure [48]. In contrast, the incorporation behavior of Mn is mainly governed by ionic size [49], and MnO_2 may undergo the following reaction during sintering [50]:

$$MnO_2 \xrightarrow{460-570\,℃} Mn_2O_3 \xrightarrow{926\,℃} Mn_3O_4 \xrightarrow{1158\,℃} MnO \tag{3}$$

Although Mn^{4+} (0.052 nm) has an ionic radius very close to that of Al^{3+} (0.057 nm), it is nearly impossible for Mn^{4+} to overcome the grain boundary energy barrier at temperatures below 570 °C. As a result, Mn^{4+} is unlikely to directly enter the lattice or substitute for Al^{3+}. On the other hand, Mn^{2+} (0.091 nm) has an absolute ionic radius difference |Δ| of approximately 59.64% compared to Al^{3+} (0.057 nm), which makes direct substitution infeasible. However, Mn^{3+} (0.066 nm) has an absolute ionic radius difference |Δ| of approximately 15.79%, allowing Mn^{3+} to partially replace Al^{3+} and form a limited solid solution. Therefore, only a small amount of Mn^{2+} exists in the mullite structure.

3.4. Evaluation and Comparison of Coal Gangue Incorporation Systems

The accumulated amount of coal gangue in China has exceeded 7 billion tons, making it the largest industrial solid waste with the most extensive land occupation. With the increasing demand for coal, the annual production of coal gangue is also growing rapidly,

reaching 330 million to 550 million tons [51], leading to a low market price of 200–300 RMB per ton. However, coal gangue contains various heavy metal elements, which, under external conditions such as weathering, erosion, and rainwater leaching, are prone to migration, causing serious environmental pollution [52]. Thermal treatment, as an economical and environmentally friendly solidification and stabilization technology, can effectively convert hazardous solid waste into harmless products [53]. Under high-temperature conditions, heavy metals can be fixed by physical encapsulation in the glass phase or by forming new chemical bonds [54]. Luo et al. [55] investigated the effect of using lead-zinc tailings and coal gangue to produce ceramic proppants. The results showed that after sintering at 1150-1250 °C, the leaching concentrations of Pb and Zn did not exceed the standard. At a sintering temperature of 1250 °C, after adding 3.0% Pb and Zn, the leaching concentrations of all samples did not exceed 0.213 mg/L, well below the Chinese standards (Pb < 5 mg/L, Zn < 100 mg/L). Peng et al. [56] prepared ceramic proppants using coal gangue and dyeing sludge and conducted heavy metal leaching tests on the ceramic before and after sintering using sulfuric and nitric acid methods. The results showed significant reductions in Cd, Cr, Cu, Ni, and Zn levels. Despite the reduction in heavy metal leaching due to thermal treatment, the issue of heavy metal leaching from coal gangue-bauxite-based ceramic proppants in underground environments still requires further attention, especially its potential impact on groundwater. Compared with coal gangue, the market price of bauxite has risen to 2850 RMB per ton. Additionally, economic analysis shows that substituting 30% coal gangue for bauxite reduces the cost

to 2070 RMB per ton, saving 27.4% on raw material costs. According to industry data, raw materials account for 30%-60% of the total cost of ceramic proppants. This substitution would lower the total cost of ceramic proppants by 8.2%-16.4%, while simultaneously alleviating the pressure of solid waste disposal. This approach offers both economic and environmental benefits for large-scale industrial applications. Therefore, this study not only enables the large-scale utilization of coal gangue but also promotes its high-value application while lowering the cost of ceramic proppants. Table 2 presents data from existing literature on the proportion of coal gangue used, sintering temperature, density, and breakage rate in ceramic proppant production using coal gangue and bauxite as raw materials. A comparative analysis shows that while the apparent density and bulk density of the ceramic proppants prepared in this study are slightly higher, their breakage rate or sintering temperature is lower than those of similar ceramic proppants. This study successfully achieves the goal of producing high-strength proppants with high coal gangue content and low energy consumption.

Conclusion

Ceramic proppants with a breakage rate below 9% were successfully produced using bauxite and calcined coal gangue as raw materials, along with 2.5–7.5 wt% composite additives of MnO_2 and TiO_2 (with a ratio of MnO_2 to TiO_2 of 3:1), within a sintering temperature range of 1250–1400 °C. Increasing the content of the composite additive promoted the development of corundum phases, the dissolution of mullite, and the formation of micropores. As the sintering temperature increased, the diffraction peak

intensities of mullite and corundum gradually became more pronounced. The ceramic proppant prepared at 1350 °C with 7.5 wt% of composite additives exhibited the best performance, presenting an apparent density of 3.17 ± 0.02 g/cm³, a bulk density of 1.88 ± 0.01 g/cm³, and a breakage rate of 2.71 ± 0.32% under 52 MPa. This study provides experimental evidence and data for the preparation of ceramic proppants utilizing composite additives.

Declaration of competing interest

The authors declare that they have no known competing financial interests or personal relationships that could have appeared to influence the work reported in this paper.

Acknowledgments

The authors acknowledge the financial support provided by The Key Program of the National Natural Science Foundation of China (Grant No.52234003) and the Australia Research Council Linkage project (LP200100420).

Appendix A. Supplementary data

The following are the supplementary data to this article:

References

[1] T.H. Kim, J.H. Lee, K.S. Lee, Integrated reservoir flow and geomechanical

model to generate type curves for pressure transient responses of a hydrauli cally-fractured well in shale gas reservoirs, J. Pet. Sci. Eng. 146 (2016) 457 -472. https://doi.org/10.1016/j.petrol.2016.06.001.

[2] Y. Tang, P.G. Ranjith, M.S.A. Perera, Major factors influencing proppant be haviour and proppant-associated damage mechanisms during hydraulic fractur ing, Acta Geotech, 13 (2018) 757-780. https://doi.org/10.1007/s11440-018-0 670-5

[3] C.T. Montgomery, M.B. Smith, Hydraulic fracturing; history of an enduring technology[J]. J. Pet. Technol,62 (2010):26-40. https://doi.org/10.2118/1210-0 026-JPT.

[4] Y. Che, Z.W. Huang, R.Y. Yang, et al., Experimental study on replacing c eramsite with quartz sand in hydraulic fracturing, Pet. Sci. Technol. 42 (202 4). https://doi.org/10.1080/10916466.2022.2143801.

[5] F.M. Michael, M.R. Krishnan, W.G. Li, et al., A review on polymer-nanofil ler composites in developing coated sand proppants for hydraulic fracturing, J. Nat. Gas Sci. Eng. 83 (2020). https://doi.org/10.1016/j.jngse.2020.103553.

[6] T.K. Guo, Y.P. Wang, Z.M. Du, et al., Evaluation of coated proppant unco nventional performance, Energy Fuels 35 (2021) 9268-9277. https://doi.org/1 0.1021/acs.energyfuels.1c00187.

[7] J. Szymanska, P. Wisniewski, P. Wawulska-Marek, et al., Determination of loamy resources impact on granulation of ceramic proppants and their prope

rties, Appl. Clay Sci. 166 (2018) 327-338. https://doi.org/10.1016/j.clay.2018.09.032.

[8] Z.J. Liao, X.G. Li, L. Ge, et al., Lightweight proppants in unconventional oil and natural gas development: A review, Sustainable. Mater. Technol. 33 (2022). https://doi.org/10.1016/j.susmat.2022.e00484.

[9] Y.Y. Yang, H. Li, Z.H. Lei, H.W. Liu, M.Y. Zeng, T.T. Yang, K.M. Chen, Y. Duan, Preparation and characterization of high-performance ceramic proppant from recycling utilization of oil-based drilling cuttings pyrolysis residues, Sci. Rep., 14 (2024). https://doi.org/10.1038/s41598-024-52334-7.

[10] X. Zhao, W.X. Li, X.R. Zhang, Y.F. Xue, J.B. Mu, D.F. Xu, W.P. Li, Y.M. Wang, S.J. Qin, Z.X. Zhang, Low-temperature preparation of lightweight ceramic proppants using high-proportioned coal-based solid wastes, Ceram. Int., 50 (2024). https://doi.org/18117-18124.10.1016/j.ceramint.2024.02.295.

[11] G.M. Li, X. Chang, B.S. Zhu, K.Y. Wang, Y. Zhou, Y.Q. Wu, Y.M. Tian, P.B. Bai, Sintering mechanism of high-intensity and low-density ceramic proppants prepared by recycling of waste ceramic sands, Adv. Appl. Ceram., 118 (2019). https://doi.org/114-120.10.1080/17436753.2018.1537204.

[12] R. Anaya, M.B. Carranza, F. Booth, M.F. Hernández, A. Mocciaro, D. Richard, N.M. Rendtorff, Low-density kaolinitic ceramic proppants based on rice husk ash, Ceram. Int., (2025). https://doi.org/10.1016/j.ceramint.2025.03.230.

[13] G.M. Li, H.Q. Ma, Y.M. Tian, et al., Feasible recycling of industrial waste

coal gangue for preparation of mullite-based ceramic proppant, Int. Conf. Se r. Mater. Sci. Nanomater. 230 (2017) 012020. https://doi.org/10.1088/1757-89 9X/230/1/012020.

[14] K.Y. Wang, H.J. Wang, Y. Zhou, Y., et al., Effect of sintering temperature on the microstructure and mechanical properties of low-cost light-weight pro ppant ceramics, Int. Conf. Mater. Sci. Nanomater. 230 (2017). https://doi.org /10.1088/1757-899X/230/1/012022.

[15] Lei Hong jiao, Tian Yuming, Song Wei, et al. Effect of Temperature on th e Performance of Low-Density Ceramic Proppants for Coalbed Methane We lls[J]. Journal of Taiyuan University of Science and Technology (In Chines e), 2023, 44(01): 57-61.

[16] Zhao Zi shi, Cui Li peng, Zhao Xu, et al. Study on the Preparation of Cer amsite Proppants Using Solid Waste Coal Gangue[J]. Shanxi Coal (In Chine se), 2019, 39(01): 1-4.

[17] J. Hao, Y. Gao, Y. Wu, et al., Preparation and characterization of low-dens ity ceramic proppant containing coal gangue additive, Mater. Res. Innovatio ns. 23 (2019) 61-65. https://doi.org/10.1080/14328917.2017.1376785.

[18] X. Zhao, Z.X. Zhang, W.X. Li, et al., Basic principle, progress, and prospe cts of coal gangue ceramic proppants, Int. J. Appl. Ceram. Technol. 20 (20 23) 2681-2699. https://doi.org/10.1111/ijac.14411.

[19] P.L. Zhao, S.H. Ma, X.H. Wang, X., et al., Properties and mechanism of

mullite whisker toughened ceramics, Ceram. Int. 49 (2023). https://doi.org/10.1016/j.ceramint.2022.11.202.

[20] D.H. Ding, W. Jiang, G.Q. Xiao, et al., Effects of CaO addition on the properties and microstructure of low-grade bauxite-based lightweight ceramic proppant, J. Aust. Ceram. Soc. 59 (2023) 957-967. https://doi.org/10.1007/s41779-023-00888-6.

[21] H. Yang, Y.L. Liu, G.L. Bai, G., et al., Solidification and utilization of water-based drill cuttings to prepare ceramsite proppant with low-density and high performance, Pet. Sci. 19 (2022) 2314-2325. https://doi.org/10.1016/j.petsci.2022.06.006.

[22] K.Z. Li, S.T. Ge, G.Q. Yuan, et al., Effects of V_2O_5 addition on the synthesis of columnar self-reinforced mullite porous ceramics, Ceram. Int. 47 (2021) 11240-11248. https://doi.org/10.1016/j.ceramint.2020.12.249.

[23] X.G. Deng, W.C. Zhang, J.Q. Yin, et al., Microstructure and mechanical performance of porous mullite ceramics added with TiO_2, Ceram. Int. 46 (2020) 8438-8443. https://doi.org/10.1016/j.ceramint.2019.12.078.

[24] Y.Y. Yang, H. Li, Z.H. Lei, et al., Preparation and characterization of high-performance ceramic proppant from recycling utilization of oil-based drilling cuttings pyrolysis residues, Sci. Rep. 14 (2024) 2314-2345. https://doi.org/10.1038/s41598-024-52334-7.

[25] M. Qin, Y.M. Tian, H.L. Hao, et al., The effect of sintering temperature o

n phase evolution and sintering mechanism of ceramic proppants with $CaCO_3$ addition, Res.-Ibero-am. J. Mater. 23 (2020). https://doi.org/10.1590/1980-5373-MR-2019-0602.

[26] H.M. Zhou, J. Li, D.Q. Yi, L.R. Xiao, Effect of Manganese Oxide on the Sintered Properties of 8YSZ, International Conference on Physics Science and Technology (ICPST)Hong Kong, PEOPLES R CHINA, 2011, pp. 14-19. https://doi.org/10.1016/10.1016/j.phpro.2011.11.005.

[27] X.D. Chen, T.H. Li, Q. Ren, X.L. Wu, H. Li, A.L. Dang, T.K. Zhao, Y.D. Shang, Mullite whisker network reinforced ceramic with high strength and lightweight, J. Alloys Compd., 700 (2017) 37-42. https://doi.org/10.1016/j.jallcom.2017.01.075.

[28] N. Montoya, F.J. Serrano, M.M. Reventós, J.M. Amigo, J. Alarcón, Effect of TiO_2 on the mullite formation and mechanical properties of alumina porcelain, J. Eur. Ceram. Soc., 30 (2010) 839-846. https://doi.org/10.1016/j.jeurceramsoc.2009.10.009.

[29] X.D. Chen, S.S. Li, Y.D. Shang, et al., In situ mullite whisker network formation for high-strength lightweight ceramic proppants, Process. Appl. Ceram., 18 (2024). https://doi.org/10.2298/PAC2401077C.

[30] S. Lahiri, S. Sinhamahapatra, H.S. Tripathi, K. Dana, Rationalizing the role of magnesia and titania on sintering of α-alumina, Ceram. Int., 42 (2016). https://doi.org/15405-15413.10.1016/j.ceramint.2016.06.189.

[31] B.X. Yang, S.J. Lu, C.H. Li, C. Fang, Y. Wan, Y.M. Lin, Reducing Water Absorption and Improving Flexural Strength of Aluminosilicate Ceramics by MnO_2 Doping, Materials, 17 (2024). https://doi.org/10.3390/ma17112557.

[32] H. Majidian, M. Farvizi, L. Nikzad, Introducing MnO_2 and ZnO Additives for the Development of Alumina-Mullite-Zirconia Composites, JOM, 73 (2021). https://doi.org/3486-3496.10.1007/s11837-021-04886-6.

[33] C.L. Gnanasagaran, K. Ramachandran, S. Ramesh, et al., Effect of co-dopin g manganese oxide and titania on sintering behaviour and mechanical prope rties of alumina, Ceram. Int., 49 (2023) 5110-5118. https://doi.org/10.1016/j. ceramint.2022.10.027.

[34] Z.L. Liu, J.Z. Zhao, Y.M. Li, et al., Y. He, Low-temperature sintering of b auxite-based fracturing proppants containing CaO and MnO_2 additives, Mate r. Lett., 171 (2016) 300-303. https://doi.org/10.1016/j.matlet.2016.02.090.

[35] Y.X. Wang, J.Z. Zhang, J.Y. Gao, et al., Modification of liquid phase and microstructure of sintered mullite by different additives, Int. J. Appl. Ceram. Technol., 22 (2025). https://doi.org/10.1111/ijac.14860.

[36] Hao Hui-lan, Gao Yun-feng, Zhu Bao-shun, et al. Study on Coal Gangue I ncorporation During Preparation of Ceramsite Proppant at Fixed Sintering T emperature[J]. Foshan Ceramics (In Chinese), 2024,34(03):51-53.

[37] Y. Jin, D. Li, Y. Liu, J. Guo, et al., Study on Pyrolysis and Oxidation Ch aracteristics of Coal Gangue Based on TGA-DSC, ACS Omega, 9 (2024) 1

4174-14186. https://doi.org/10.1021/acsomega.3c09743.

[38] Y. Jin, D. Li, Y. Liu, et al., X. Yan, Study on Pyrolysis and Oxidation Ch aracteristics of Coal Gangue Based on TGA-DSC, ACS Omega, 9 (2024) 1 4174-14186. https://doi.org/10.1021/acsomega.3c09743.

[39] Y.Y. Zhang, L. Xu, S. Seetharaman, et al., Effects of chemistry and minera l on structural evolution and chemical reactivity of coal gangue during calci nation: towards efficient utilization, Mater. Struct., 48 (2015) 2779-2793. htt ps://doi.org/10.1617/s11527-014-0353-0.

[40] S. Shao, B.Z. Ma, C.Y. Wang, et al., Thermal behavior and chemical reacti vity of coal gangue during pyrolysis and combustion, Fuel, 331 (2023). http s://doi.org/10.1016/j.fuel.2022.125927.

[41] Z.H. Guo, J.J. Xu, Z.H. Xu, et al., Performance of cement-based materials containing calcined coal gangue with different calcination regimes, J. Build. Eng., 56 (2022). https://doi.org/10.1016/j.jobe.2022.104821.

[42] W.C. Krumbein, Measurement and geological significance of shape and roun dness of sedimentary particles, J. Sediment. Res., 11 (1941) 64-72. https://d oi.org/10.1306/d42690f3-2b26-11d7-8648000102c1865d.

[43] J.F. Gu, J. Zou, J.H. Liu, et al., Sintering highly dense ultra-high temperatu re ceramics with suppressed grain growth, J. Eur. Ceram. Soc., 40 (2020) 1 086-1092. https://doi.org/10.1016/j.jeurceramsoc.2019.11.056.

[44] D.H. Ding, W. Jiang, G.Q. Xiao, et al., Effects of CaO addition on the pro

perties and microstructure of low-grade bauxite-based lightweight ceramic pr oppant, J. Aust. Ceram. Soc., 59 (2023) 957-967. https://doi.org/10.1007/s41 779-023-00888-6.

[45] S.H. Wang, W. Yan, J.J. Yan, et al., Microstructures and properties of micr oporous mullite-corundum aggregates for lightweight refractories, Int. J. App l. Ceram. Technol., 19 (2022) 3300-3310. https://doi.org/10.1111/ijac.14123.

[46] M. Qin, Y.M. Tian, H.L. Hao, et al., Effects of $CaCO_3$ additive on properti es and microstructure of corundum- And mullite-based ceramic proppants, In t. J. Appl. Ceram. Technol., 17 (2020) 1026-1032. https://doi.org/10.1111/ija c.13470.

[47] Y.-F. Chen, M.-C. Wang, M.-H. Hon, Secondary Mullite Formation in Kaol in – Al_2O_3 Ceramics, J. Mater. Res., 19 (2004) 806-814. https://doi.org/10.15 57/jmr.2004.19.3.806.

[48] H. Schneider, R.X. Fischer, J. Schreuer, Mullite: Crystal Structure and Relat ed Properties, J. Am. Ceram. Soc., 98 (2015) 2948-2967. https://doi.org/10.1 111/jace.13817.

[49] H. Schneider, J. Schreuer, B. Hildmann, Structure and properties of mullite - A review, J. Eur. Ceram. Soc., 28 (2008) 329-344. https://doi.org/10.1016/ j.jeurceramsoc.2007.03.017.

[50] M. Feng, Y.Q. Wu, G.R. Ji, et al., Sintering mechanism and properties of corundum-mullite duplex ceramic with MnO_2 addition, Ceram. Int., 48 (202

2) 14237-14245. https://doi.org/10.1016/10.1016/j.ceramint.2022.01.312.

[51] C.G. Wang, D.M. Wang, H.H. Xin, et al., Study on secondary oxidation ch aracteristics of coal gangue at different pyrolysis rank, Fuel, 345 (2023). htt ps://doi.org/10.1016/10.1016/j.fuel.2023.128231.

[52] B.F. Zhang, K. Yang, K. Zhang, Q.B. Wang, N.Q. Wu, Migration transformation, prevention, and control of typical heavy metal lead in coal gangue: a review, Int. J. Coal Sci. Technol., 10 (2023). https://doi.org/10.1007/s40789-023-00656-8.

[53] B. Gonzá lez-Corrochano, J. Alonso-Azcá rate, M. Rodas, Effect of thermal treatment on the retention of chemical elements in the structure of lightweight aggregates manufactured from contaminated mine soil and fly ash, Constr. Build. Mater., 35 (2012) 497-507. https://doi.org/10.1016/j.conbuildmat.2012.04.061.

[54] K. Krausova, L. Gautron, A. Karnis, G. Catillon, S. Borensztajn, Glass ceramics and mineral materials for the immobilization of lead and cadmium, Ceram. Int., 42 (2016) 8779-8788. https://doi.org/10.1016/j.ceramint.2016.02.119.

[55] Z.T. Luo, J.Y. Guo, X.H. Liu, Y.D. Mu, M.X. Zhang, M. Zhang, C.F. Tian, J.H. Ou, J. Mi, Preparation of ceramsite from lead-zinc tailings and coal g angue: Physical properties and solidification of heavy metals, Constr. Build. Mater., 368 (2023). https://doi.org/10.1016/j.conbuildmat.2023.130426.

[56] C. Peng, G.F. Dai, Y.H. Wang, J.H. Yang, C.X. Wang, S. Jiao, L. Chen, C. L. Duan, P. Li, Preparation of high-strength ceramsite from coal gangue and printing and dyeing sludge: Design strategy and modelling mechanism, Cer

am. Int., 50 (2024) 19963-19970. https://doi.org/10.1016/j.ceramint.2024.03.122.

[57] J.Y. Hao, H.Q. Ma, X. Feng, et al., Microstructure and fracture mechanism of low density ceramic proppants, Mater. Lett., 213 (2018) 92-94. https://doi.org/10.1016/j.matlet.2017.11.021.

[58] J.Y. Hao, H.L. Hao, Y.F. Gao, et al., Wang, Effect of Sintering Temperature on Property of Low-Density Ceramic Proppant Adding Coal Gangue, Materials Science-Medziagotyra, 26 (2020) 94-98. https://doi.org/10.5755/j01.ms.26.1.19376.

Table 1 Chemical Composition of Raw Materials (wt%)

	Al_2O_3	SiO_2	TiO_2	Fe_2O_3	K_2O	CaO	MgO	other
Bauxite	77.675	13.138	5.407	1.385	1.066	0.271	0.268	0.79
Coal Gangue	32.246	48.163	0.653	5.892	2.254	0.384	0.392	10.016
Calcined Coal Gangue	34.13	51.66	0.57	8.44	2.42	0.37	0.312	2.098

Table 2 Comparison of Coal Gangue-Based Ceramic Proppants Prepared with Composite Additives and Those Reported in Literature

Raw materials	Sintering temperature (°C)	Additives/wt%	Apparent density(g/cm^3)	Bulk density(g/cm^3)	Breakage ratio(%)	Refs.
Bauxite coal gangue	1350	$CaCO_3$	3.10	1.42	8.41(52MPa)	[24]
Bauxite coal gangue	1250	Magnesia slag/3	-	-	7.64(52MPa)	[57]
Bauxite coal gangue	1400	Feldspar, dolomite TiO_2/12	-	1.36	2.19(52MPa)	[29]
Bauxite coal gangue	1450	-	2.85	1.54	6.8(35MPa)	[13]
Calcined firestone clay coal gangue	1400	-	2.79%	1.27	8.36(52MPa)	[58]
Bauxite coal gangue	1350	MnO_2, TiO_2 /7.5	3.17	1.88	2.71(52MPa)	This work
	1250		3.12	1.72	7.35(52MPa)	

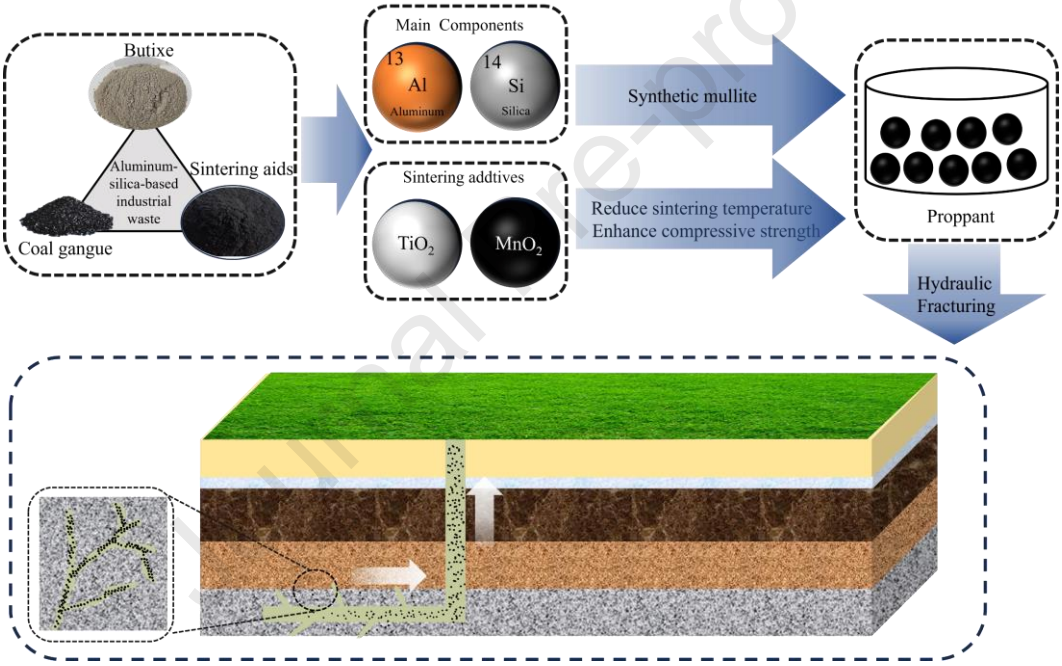

Figure 1 Process Strategy Diagram for Preparing Ceramic Proppants from Coal Gangue Waste.

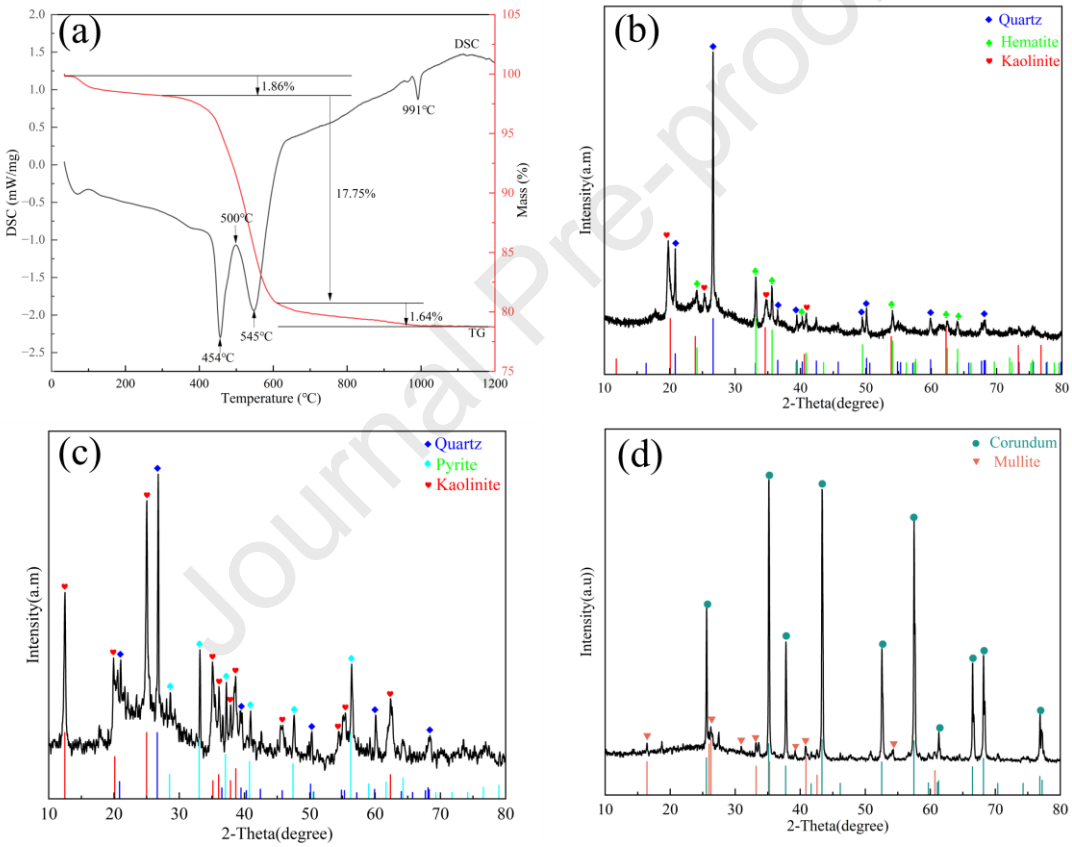

Figure 2 (a) TG–DSC curve of raw coal gangue. (b) XRD pattern of raw coal gangue. (c) XRD pattern of coal gangue calcined at 700 °C. (d) XRD pattern of bauxite

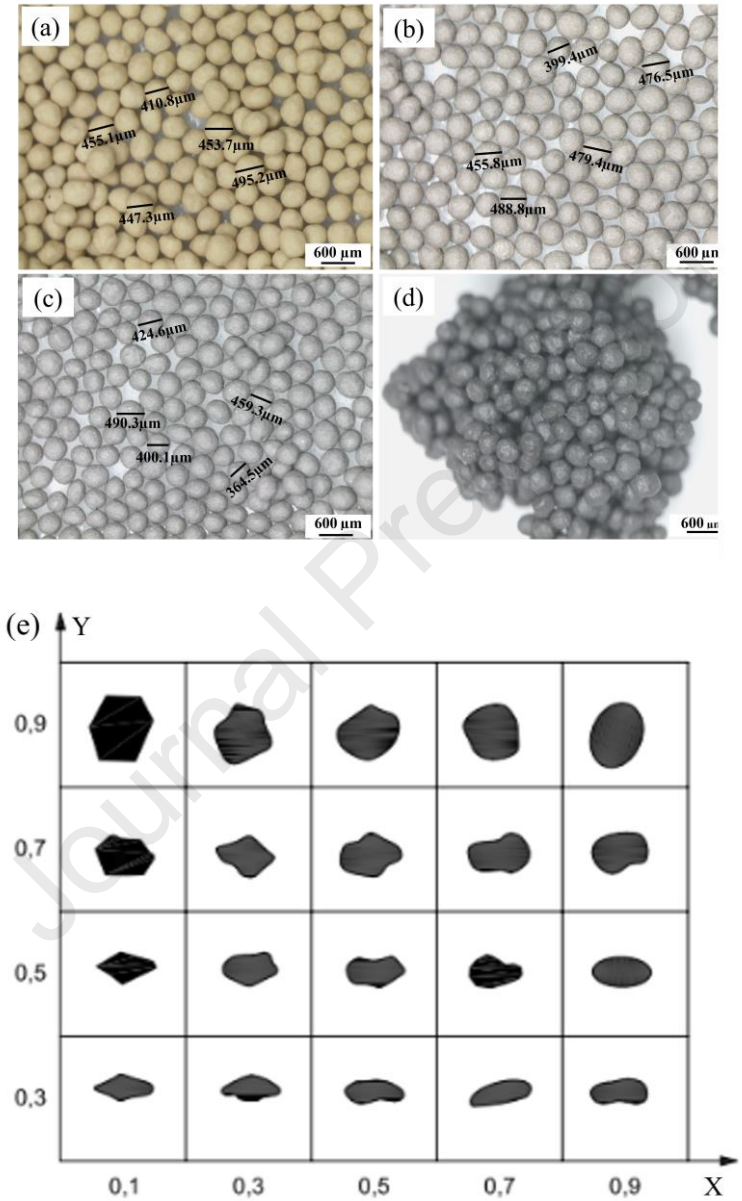

Figure 3 Macroscopic morphology of Z1-Z4 ceramic proppants and the Krumbein/Slos template. (a) Z1, (b) Z2, (c) Z3, (d) Z4, (e) Krumbein/Slos template

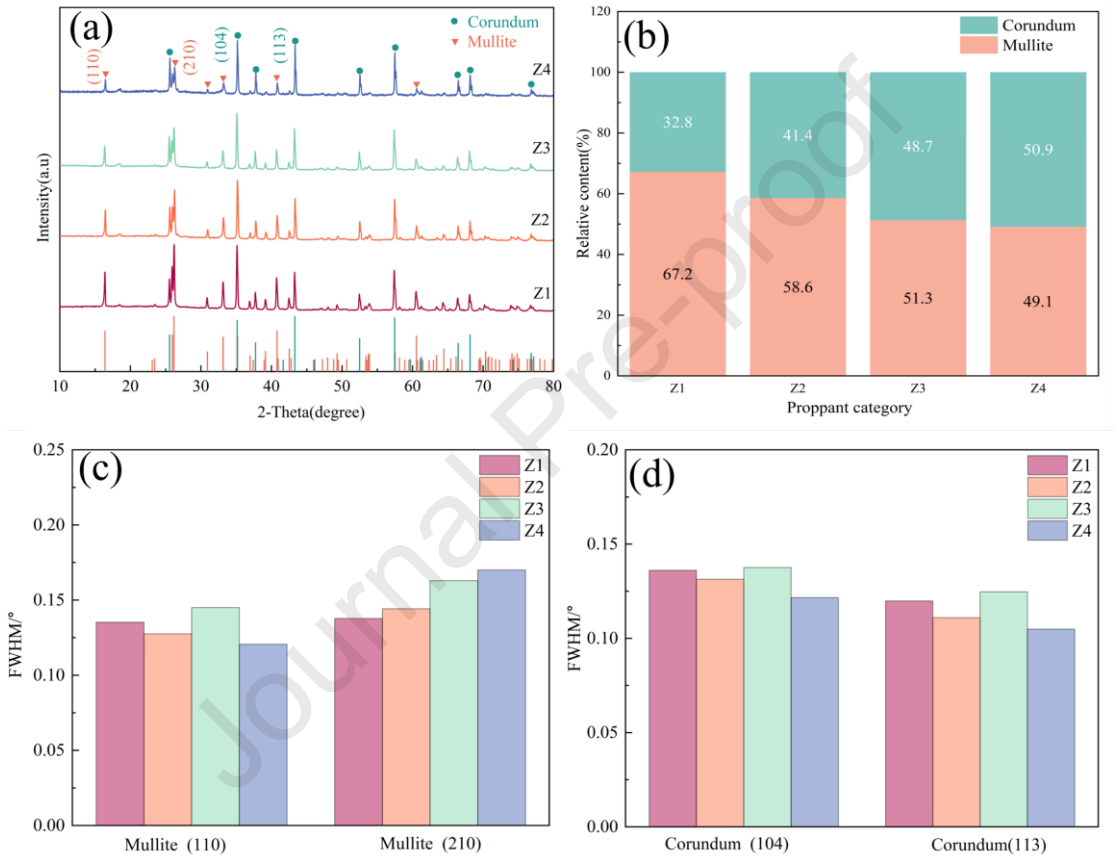

Figure 4 XRD characterization and phase composition of ceramic proppant samples Z1-Z4. (a) XRD patterns of ceramic proppant Z1-Z4. (b) Semi-quantitative analysis of mullite and corundum phases in Z1-Z4. (c) FWHM of the mullite diffraction peaks in Z1-Z4. (d) FWHM of the corundum diffraction peaks in Z1-Z4.

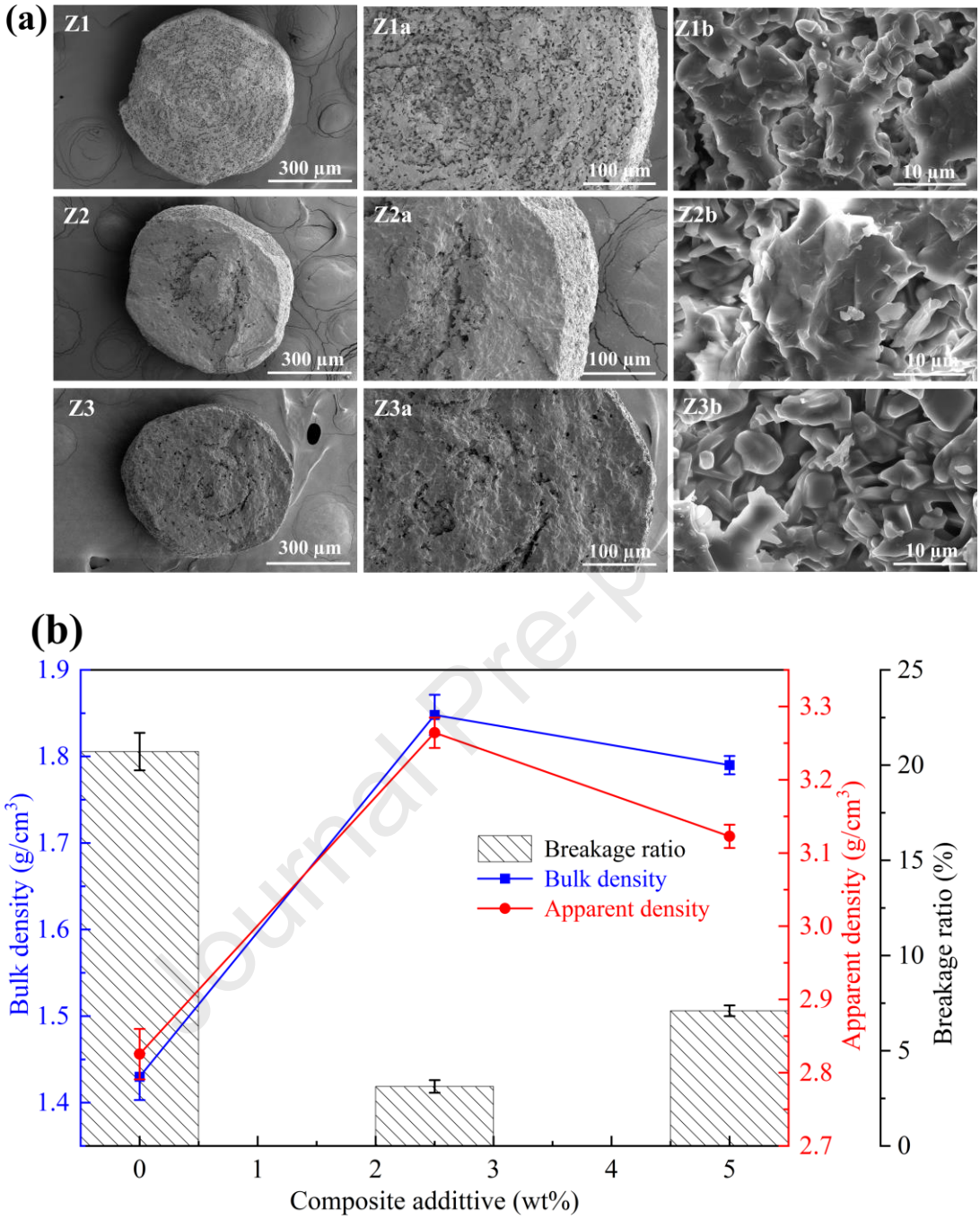

Figure 5 Microstructural and Performance Characterization of Ceramic Proppants Z1-Z3. (a) Cross-sectional SEM images of ceramic proppants Z1–Z3; (b) Comparison of bulk density, apparent density, and breakage rate of Z1–Z3.

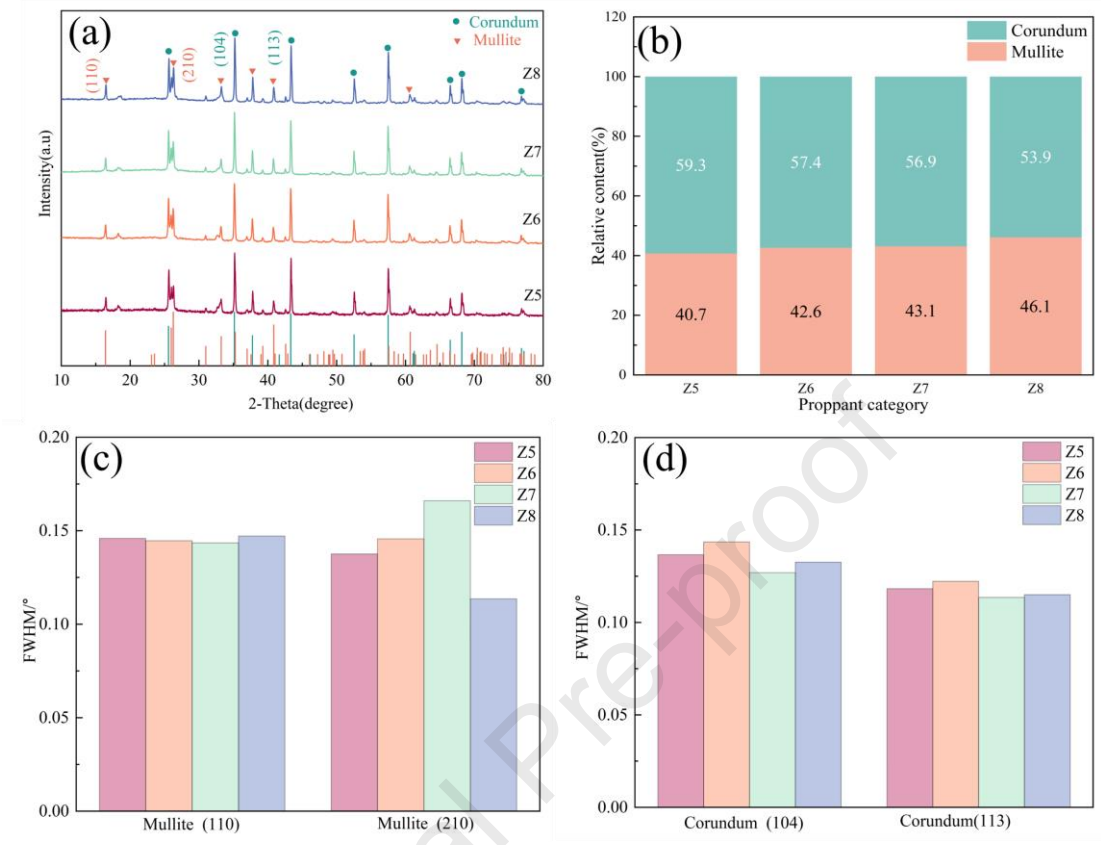

Figure 6 XRD characterization and phase composition of ceramic proppant samples Z5-Z8. (a) XRD patterns of ceramic proppant Z5-Z8. (b) Semi-quantitative analysis of mullite and corundum phases in Z5-Z8. (c) FWHM of the mullite diffraction peaks in Z5-Z8. (d) FWHM of the corundum diffraction peaks in Z5-Z8.

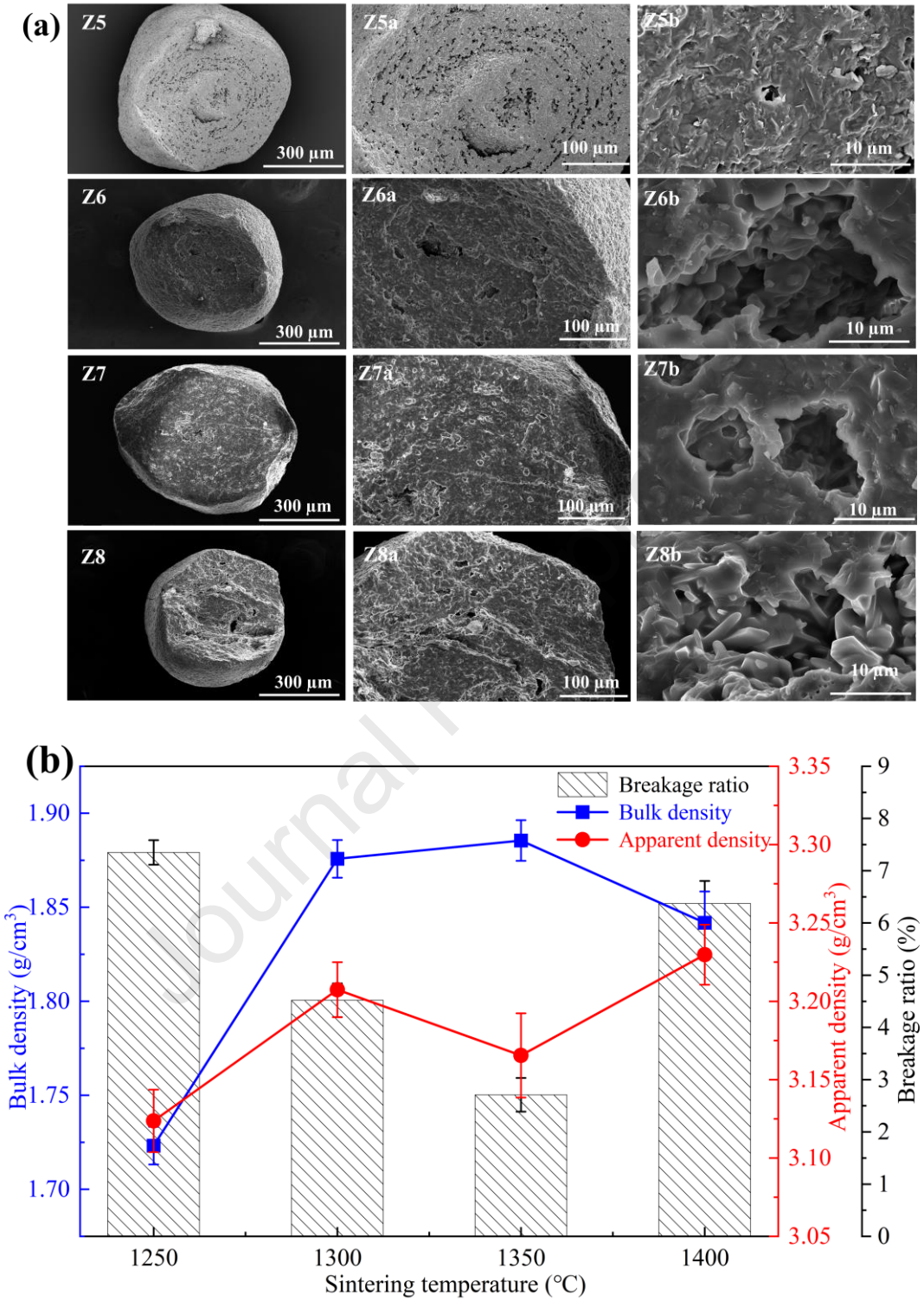

Figure 7 Microstructural and Performance Characterization of Ceramic Proppants Z5–Z8. (a) Cross-sectional SEM images of ceramic proppants Z5–Z8;(b) Comparison of bulk density, apparent density, and breakage rate of Z5–Z8.

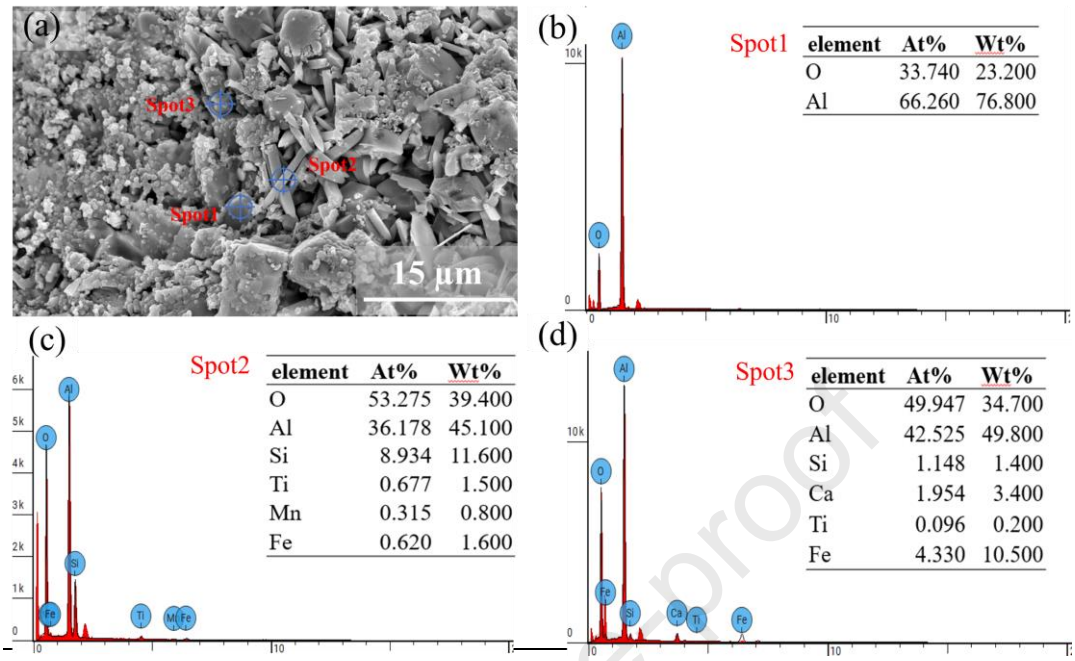

Figure 8 SEM and EDS spectra of Z7 ceramic proppant after 3% HF treatment

Supporting information

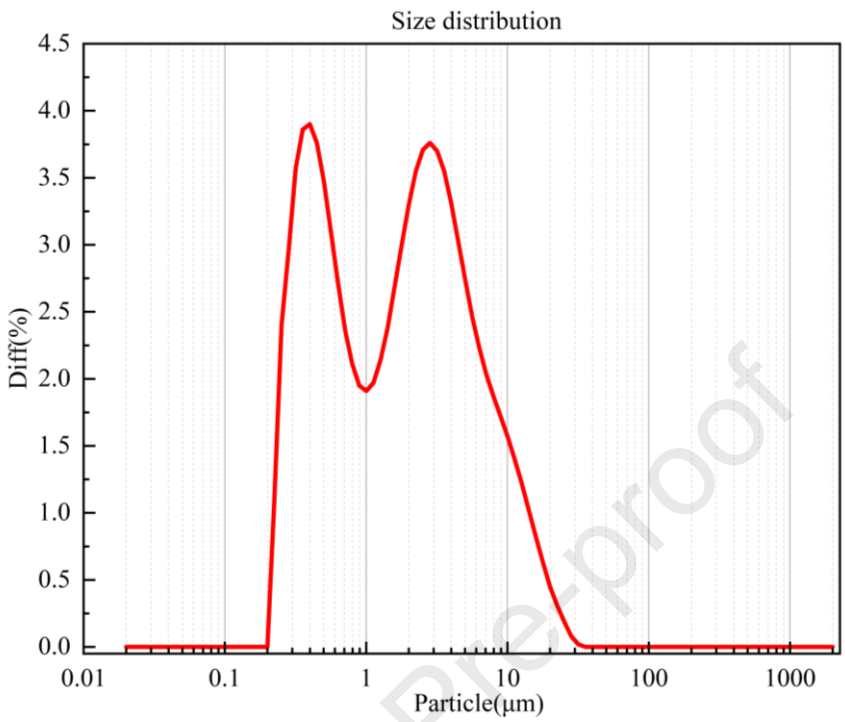

Figure S1. Particle size distribution of mixed materials after 4 h of ball milling.

Table S1. Composition ratio of proppant specimens

	bauxite（wt%）	Coal ganaue(wt%)	MnO_2+TiO_2(wt%)	Sintering temperature(℃)
Z1	70	30	0	1450
Z2	68.25	29.25	2.5	1450
Z3	66.5	28.5	5	1450
Z4	64.75	27.75	7.5	1450
Z5	64.75	27.75	7.5	1250
Z6	64.75	27.75	7.5	1300
Z7	64.75	27.75	7.5	1350
Z8	64.75	27.75	7.5	1400

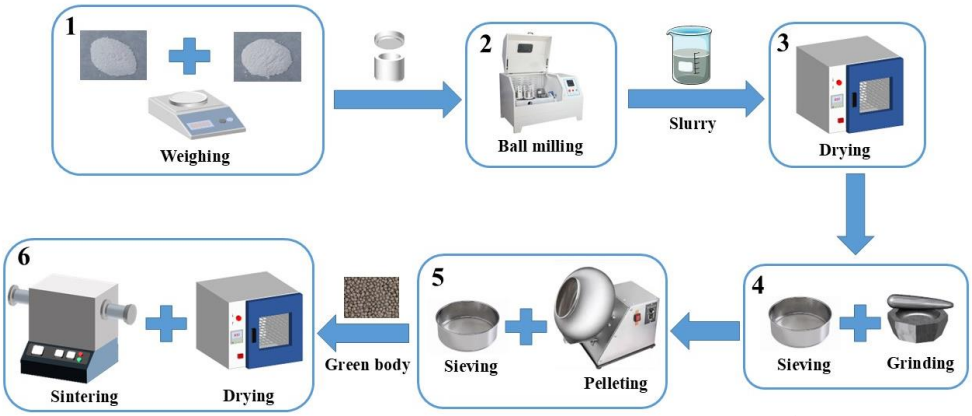

Figure S2. Fabrication process of ceramic proppant.

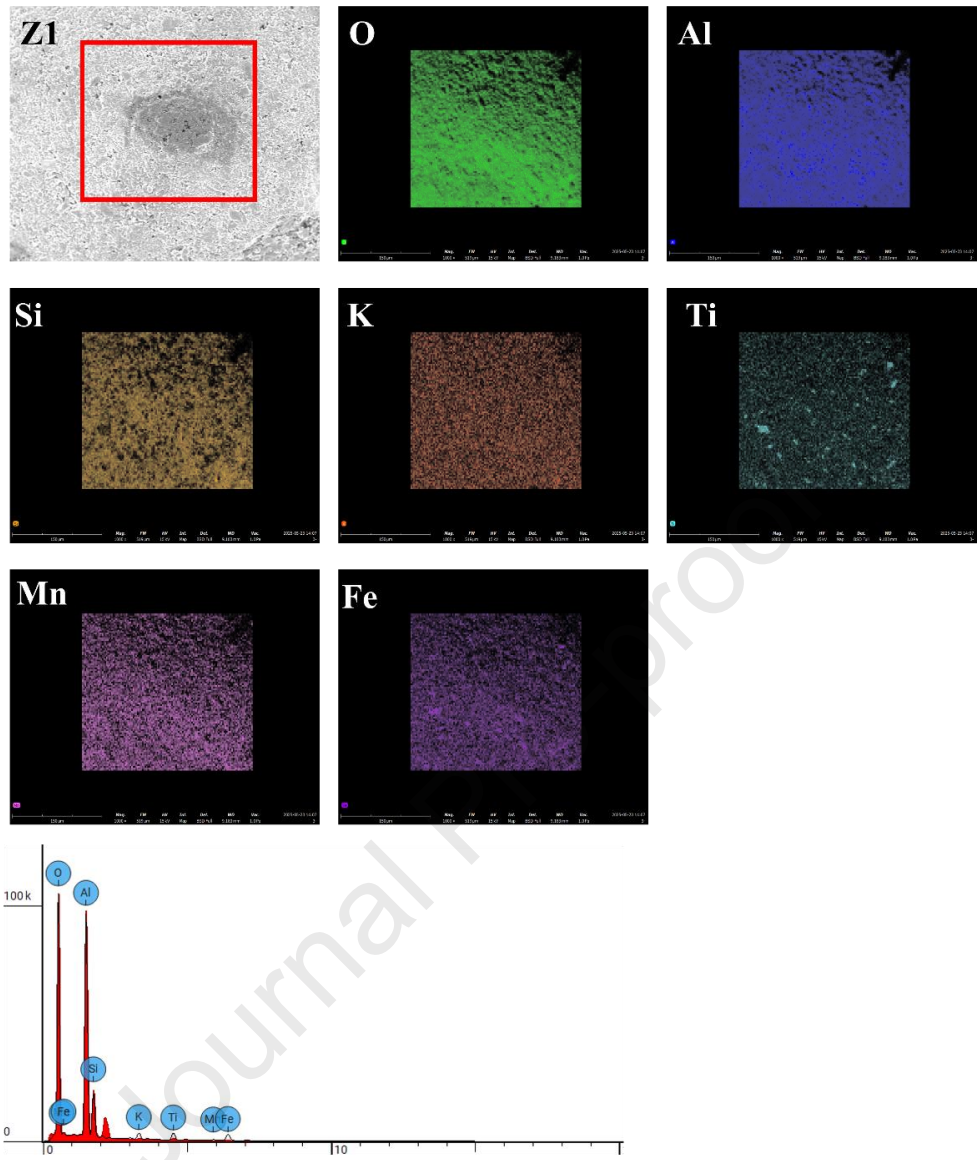

Element Symbol	Element Name	Atomic Conc.	Weight Conc.
O	Oxygen	59.972	44.444
Al	Aluminum	29.488	36.837
Si	Silicon	5.462	7.107
K	Potassium	1.327	2.402
Ti	Titanium	1.308	2.903
Mn	Manganese	0.275	0.701
Fe	Iron	2.167	5.606

Figure S3. Cross-sectional EDS mapping and semi-quantitative elemental analysis

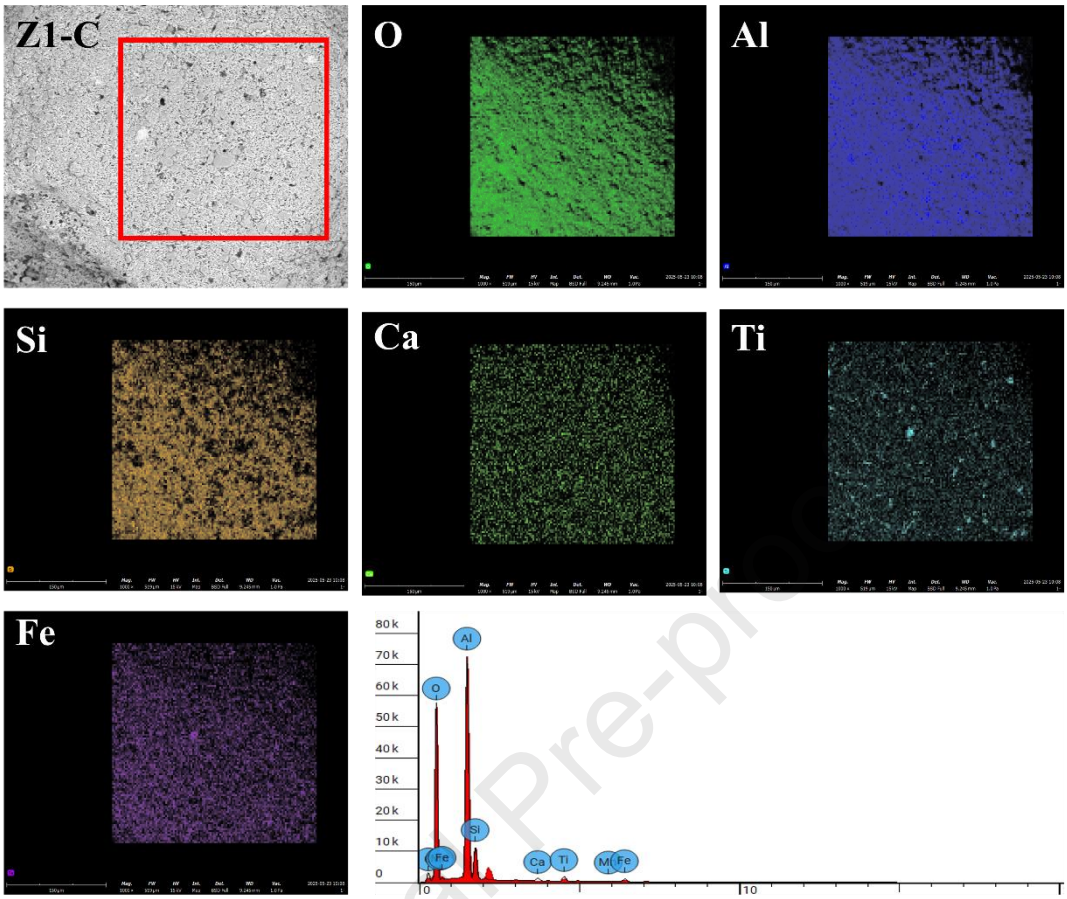

Element Symbol	Element Name	Atomic Conc.	Weight Conc.
O	Oxygen	50.559	40.500
Al	Aluminum	37.892	39.500
Si	Silicon	9.124	5.800
Ca	Calcium	0.548	1.100
Ti	Titanium	0.876	2.100
Mn	Manganese	0.000	0.000
Fe	Iron	1.001	2.800

Figure S4. Cross-sectional EDS mapping and semi-quantitative elemental analysis of the Z1 proppant after corrosion.

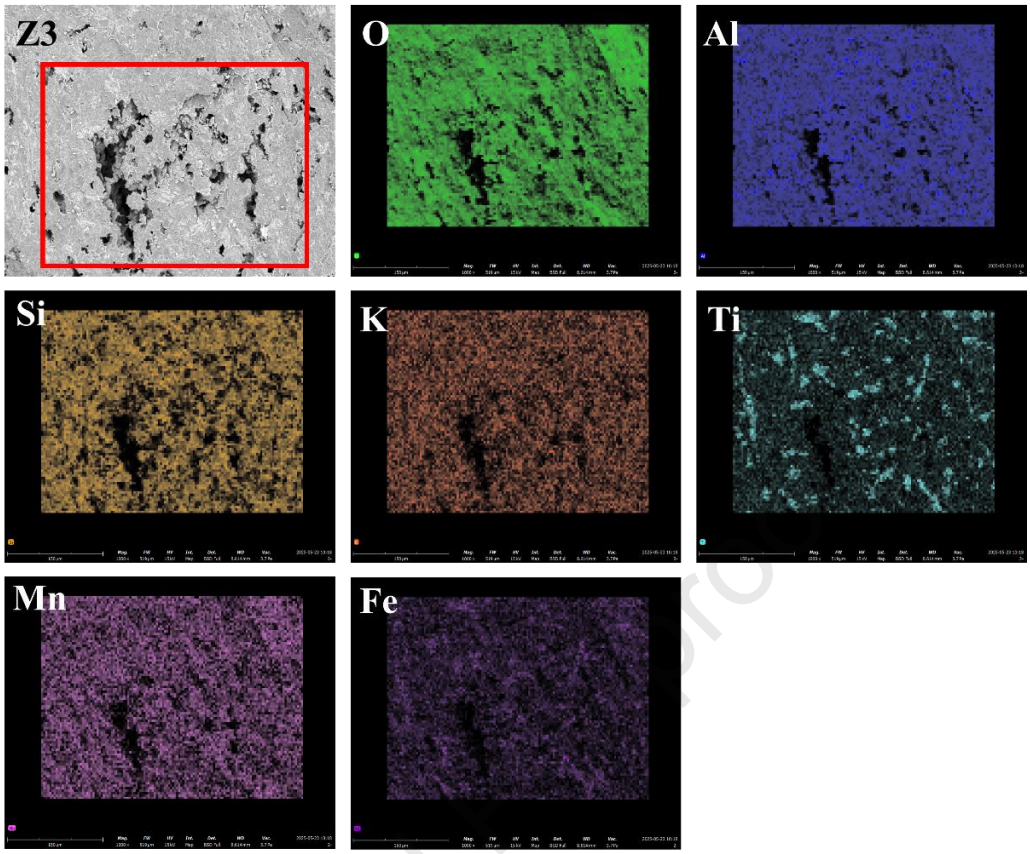

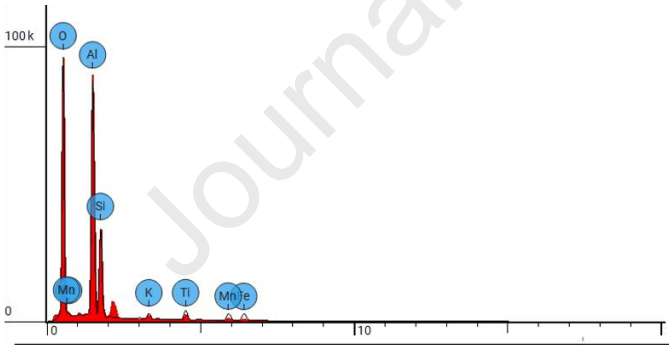

Element Symbol	Element Name	Atomic Conc.	Weight Conc.
O	Oxygen	57.046	40.841
Al	Aluminum	27.373	33.033
Si	Silicon	9.238	11.612
K	Potassium	0.973	1.702
Ti	Titanium	1.495	3.203
Mn	Manganese	1.832	4.505
Fe	Iron	2.043	5.105

Figure S5. Cross-sectional EDS mapping and semi-quantitative elemental analysis

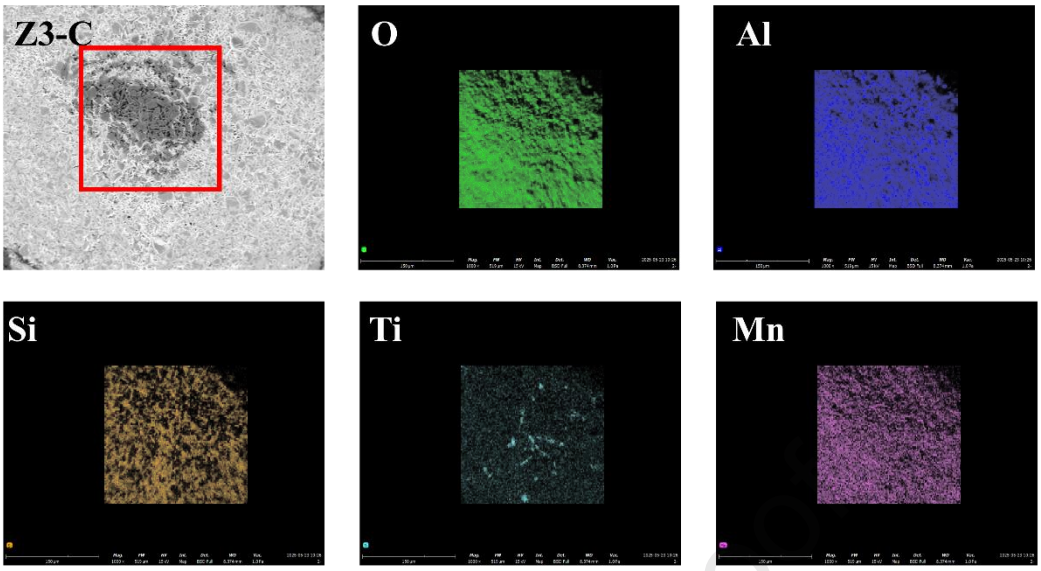

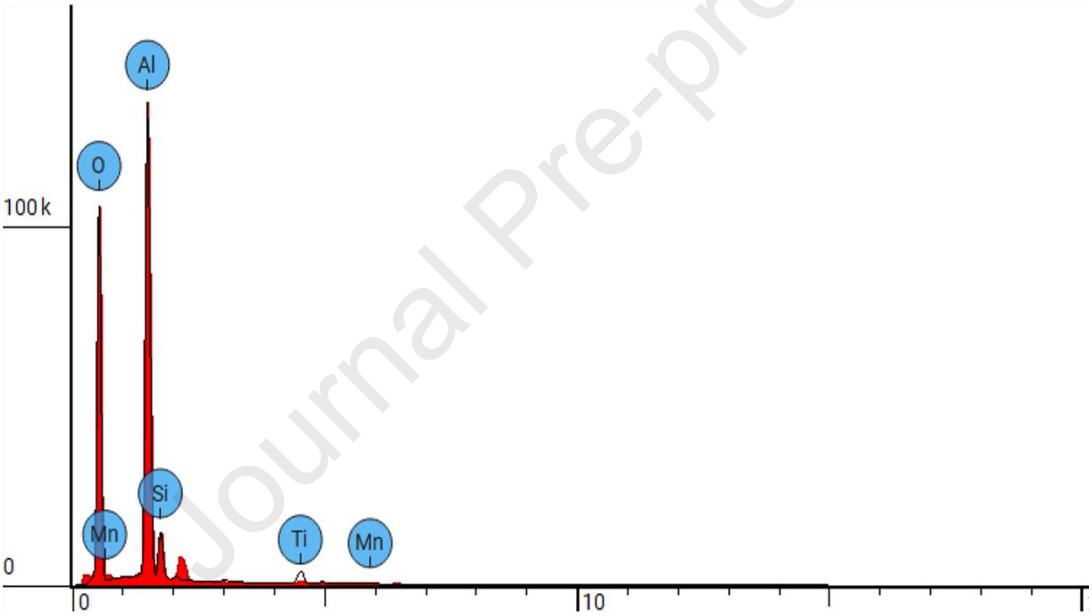

Element Symbol	Element Name	Atomic Conc.	Weight Conc.
O	Oxygen	57.447	43.600
Al	Aluminum	36.973	47.300
Si	Silicon	3.903	5.200
Ti	Titanium	1.408	3.200
Mn	Manganese	0.269	0.700

Figure S6. Cross-sectional EDS mapping and semi-quantitative elemental analysis

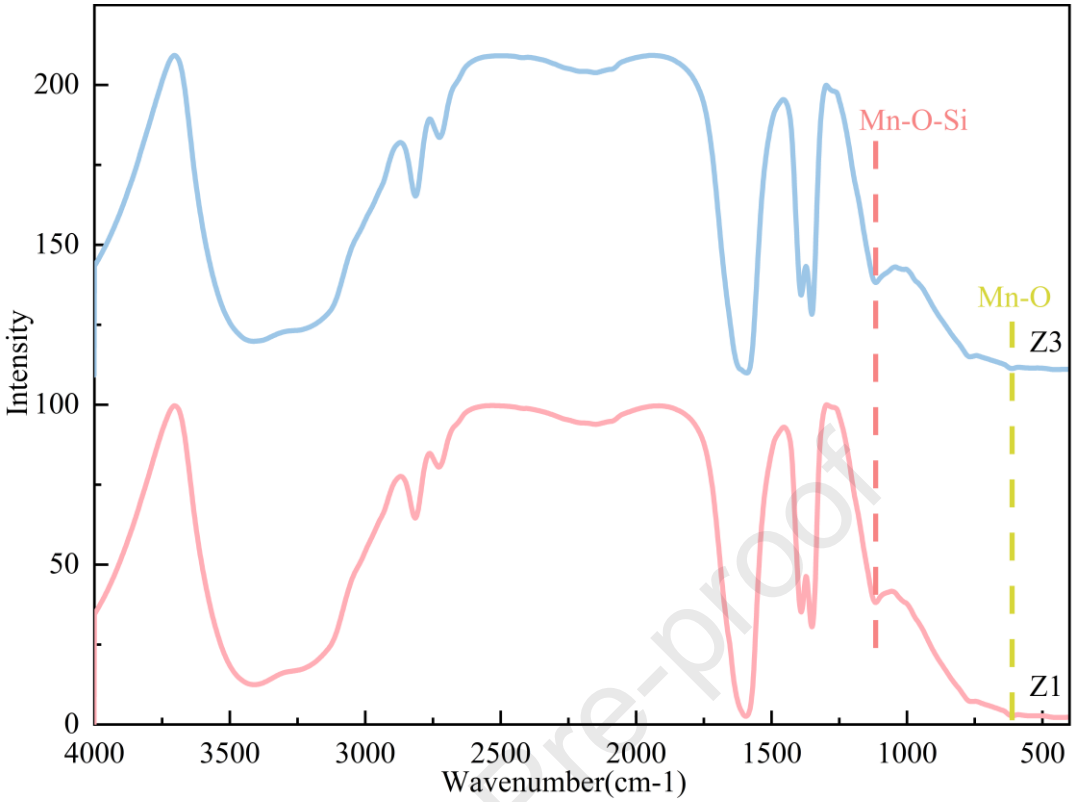

Figure S7. FTIR spectra of samples Z1 and Z3.

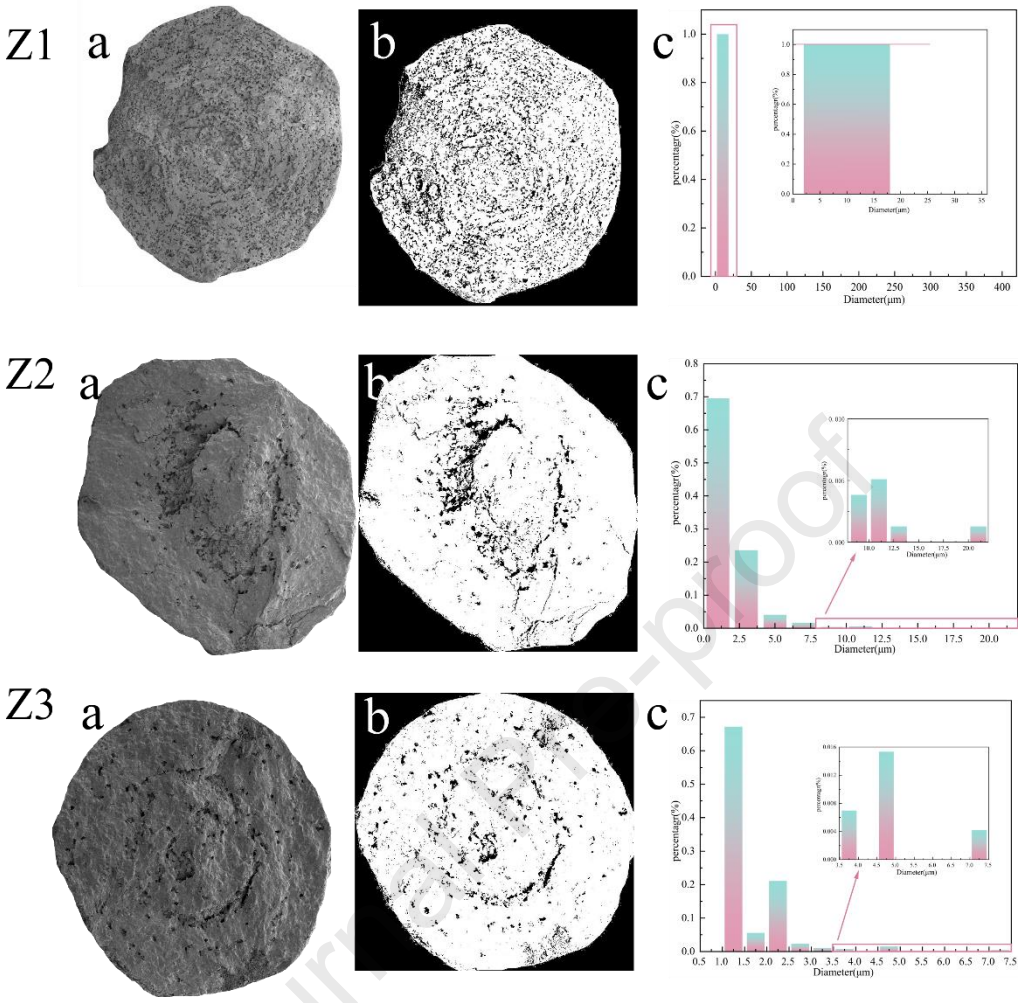

Figure S8. Pore size analysis of Z1-Z3 proppants: (a) SEM cross-sectional image, (b) Pore analysis results, (c) Pore size distribution chart.

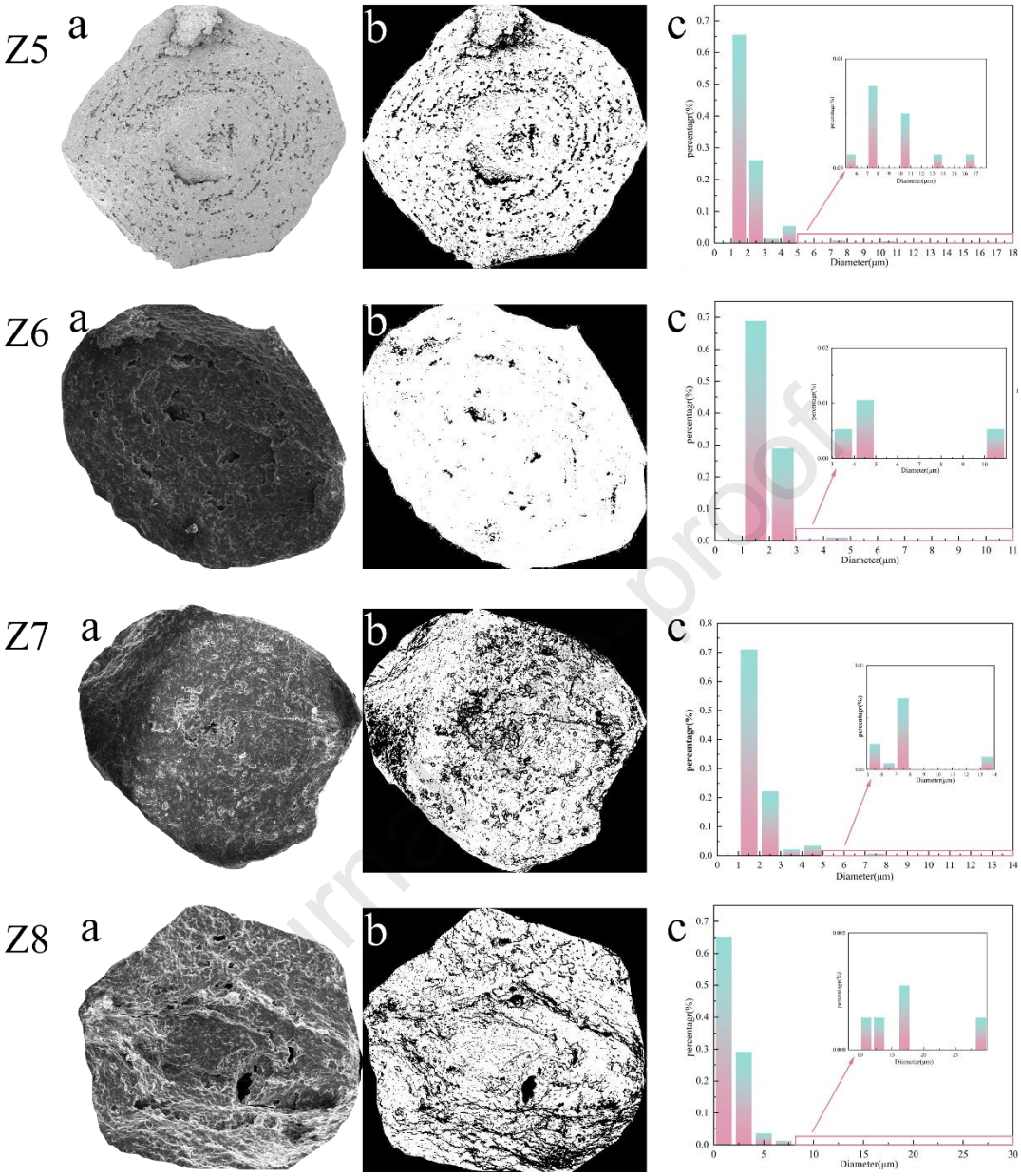

Figure S9. Pore size analysis of Z5-Z8 proppants: (a) SEM cross-sectional image, (b) Pore analysis results, (c) Pore size distribution chart.

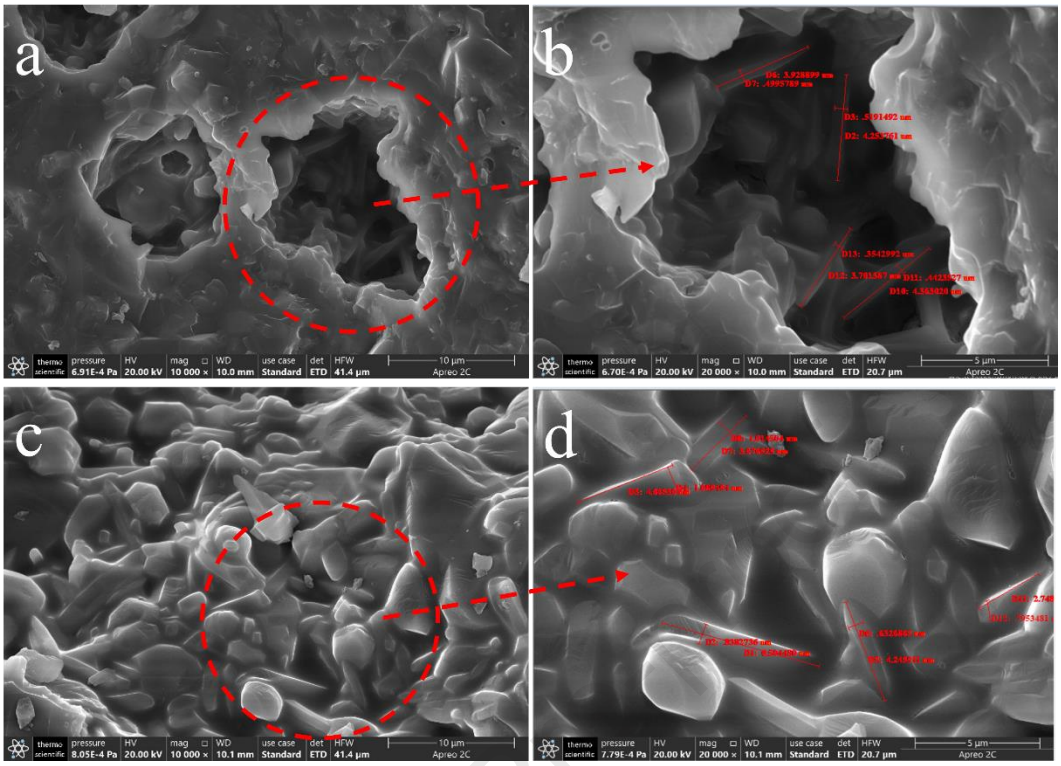

Figure S10. SEM images of Z7 and Z8 proppants: (a) Z7 at 10,000× magnification, (b) Z7 at 20,000× magnification, (c) Z8 at 10,000× magnification, and (d) Z8 at 20,000× magnification.

Declaration of interests

☒ The authors declare that they have no known competing financial interests or personal relationships that could have appeared to influence the work reported in this paper.

☐The authors declare the following financial interests/personal relationships which may be considered as potential competing interests: